

The Timing of Global Floods and its Association with Climate and Topography

Paula Torre Zaffaroni¹, German Baldi², Marcos Texeira³, Carlos Marcelo Di Bella¹, and Esteban Gabriel Jobbagy⁴

¹Instituto de Investigaciones Fisiológicas y Ecológicas Vinculadas a la Agricultura

²Instituto de Matemática Aplicada San Luis

³IFEVA (Agricultural Plant Physiology and Ecology Research Institute)

⁴IMASL - Universidad Nacional de San Luis/CONICET

April 6, 2023

Abstract

Until recently, the development of a global geography of floods was challenged by the fragmentation and heterogeneity of in situ data and the high costs of processing large amounts of remote sensing data. Such geography would facilitate the exploration of large-scale drivers of flood extent and timing including wide latitudinal, climate, and topographic effects. Here we used a monthly dataset spanning 30 years (Global Surface Water Extent) to develop a worldwide geographical characterization of slow floods (1-degree grid), weighting the relative contribution of seasonal, interannual, and long-term fluctuations on overall variability, and quantifying precipitation-flooding delays where seasonality dominated. We explored the dominance of different flooding timings across five Köppen-Geiger main climates and seven topography classes derived from modeled water table depths (i.e., hydro-topography) to contribute top-down insight about the outstanding, cross-regional flooding patterns and their likely large-scale drivers. Our results showed that, globally, the mean extent of floods averaged 0.48% of the global land area, predominantly associated with hydro-topography (>2x more extensive in flatter landscapes). Climate drove flood timings, with predictable, seasonally-dominated fluctuations in cold regions, interannual and mixed patterns in temperate climates, and more irregular (higher variability) and unpredictable (less seasonal) patterns in arid regions. Net gains of flooded area dominated temporal variability in 9% of the cells including boreal clusters likely affected by warming trends. We propose that this new geographical perspective of floods can aid different avenues of hydrological research in the upscaling and extrapolation of field studies and the parsimonious representation of floods in hydroclimatic models.

1 Introduction

Floods influence a myriad of biophysical and human processes at multiple spatial and temporal scales, examples of which are nutrient cycles in riverine environments, primary productivity and ecological succession in wetlands, and local climate properties (Aufdenkampe et al., 2011; Davies et al., 2008; Faysse et al., 2020; Houspanossian et al., 2018; Jardine et al., 2015; Robertson et al., 2001; Sanchis et al., 2012; Simões et al., 2013; Loarie et al., 2011). The temporal dynamics of floods modulate these influences and may be described according to regimes and timings. Flood regimes have been defined through their association with different triggers, i.e., rainfall pulses, snowmelt, runoff from upslope areas, and soil moisture (R. Merz & Blöschl, 2003; Parajka et al., 2010), and through the level of sensitivity to terrain or atmospheric properties, i.e., hydraulic infrastructure, land use and land cover changes, and climatic changes (Sivapalan, 2005; Prigent et al., 2007; Silva et al., 2017; B. Merz et al., 2021). Flood timing, instead, describes the moment, duration, and degree of periodicity of flooding peaks (e.g. summer vs. winter-time floods, flash floods lasting days vs. slow floods lasting months, seasonal vs. erratic floods). It is also characterized according to their recurrence and degree of extremeness (e.g., 1- vs. 100-year), and rich/poor flooding periods lasting several years (Cunderlik et al., 2004; Hall et al., 2014; Lee et al., 2015; R. Merz & Blöschl, 2003; Pickens et al., 2020; Saharia et al., 2017; Tulbure & Broich, 2019; Warfe et al., 2011). Thus, and from a systems theory framework (O’Neill et al., 1986), we could distinguish scale-dependent factors influencing these two aspects of flooding dynamics. From a bottom-up perspective, we can view flooding regimes as the result of different processes (i.e., causal mechanisms). In turn, from a top-down perspective, we can think of the dominating timescale at which flooding fluctuates (hereby, flood timing; for example, seasons, years and even decades) as indicators of the influence of drivers that (i) operate at larger spatial scales (e.g., climate regimes, atmospheric circulation patterns) (Kundzewicz et al., 2019), and (ii) are particularly susceptible to the many ongoing anthropogenic changes (Trenberth, 2011). To improve our understanding of the dominant drivers of floods, it becomes fundamental to weigh and explain the temporal attributes of flooding across large scales.

70 While our current knowledge of the drivers of floods at large spatial and tempo-
71 ral scales has been growing with the increasing availability of historical data and paleo-
72 oenvironmental proxies (Blöschl et al., 2020; Knox, 2000) together with modern remote
73 sensing information (Alsdorf et al., 2007; C. Huang et al., 2018; Lopez et al., 2020), a
74 comprehensive understanding of the drivers of flooding at the global level is still miss-
75 ing. Indeed, hierarchically bottom-up, causal mechanisms (i.e., processes, such as soil
76 moisture excess after exceeding its infiltration capacity) answering to upper-level drivers
77 have been described from local (Troch et al., 1994; Arora et al., 2021; Alborzi et al., 2022)
78 to catchment (Delgado et al., 2012; Ganguli et al., 2020; Jencso & McGlynn, 2011) and
79 continental levels (Hall et al., 2014; Blöschl et al., 2017; McCabe et al., 2007), yet the
80 larger, global patterns remain underexplored. A mismatch, arising from incongruences
81 in spatial, temporal, and methodological approximations, has been found between the
82 many lines of hydrology research across the planet (Rogger et al., 2017), that constrains
83 the possibilities to upscale from local processes to global patterns (Blöschl, 2006). It might
84 be partly for these reasons that global models still show high uncertainty in anticipat-
85 ing how floods may shift under the conjunct effects of climate change, land cover change,
86 and infrastructure development. A uniform characterization of the timing and extent of
87 floods at the global level and its link with regional drivers is the first step towards the
88 improvement of global flooding modeling.

89 To this day, global efforts quantifying the temporal dynamics of floods have gone
90 a long way into describing very local (e.g., 900 m²)- to basin-level variance at different
91 timescales, but have not explored geographical patterns or the drivers to aid their in-
92 terpretation. Two main lines of research can be distinguished. First, classifications of
93 continental surface water based on remote sensing information have been able to char-
94 acterize, to different extents, flooding dynamics for a few years (Cao et al., 2014; Pri-
95 gient et al., 2007) to up to 35 years (Pekel et al., 2016a; Pickens et al., 2020). Their quasi-
96 complete global coverage has allowed the identification of long-term change (over 10 to
97 35 years) hotspots associated with water infrastructure and climate change effects (Pekel
98 et al., 2016a), and the correlation between rainfall and floods over latitudinal belts (Prigent
99 et al., 2007) and climate regimes (e.g., temperature and precipitation, Cao et al., 2014),
100 among other large-scale questions that can be addressed with these tools. However, nei-
101 ther discuss the existence of geographical patterns of flood timing that could arise from
102 their findings (e.g., across continents, latitudinal and/or longitudinal gradients). Second,
103 recom compilations of streamflow records of up to 70 years have given place to detailed clas-
104 sifications of flood season patterns (Do et al., 2020; Lee et al., 2015; B. Merz et al., 2021;
105 Stein et al., 2020), yet the heterogeneous distribution of gauging stations hampers their
106 extrapolation capacity to ungauged catchments and continents (e.g., South America, South
107 Asia, and Africa). Ultimately, global studies have advanced in the classification of floods
108 and the identification of temporal patterns, but their ability to upscale their conclusions
109 on global drivers remains limited due to (i) lack of pattern recognition, (ii) short time
110 periods of observation; and/or (iii) geographically-biased data availability.

111 In turn, our deepest understanding of large-scale flooding dynamics comes from ob-
112 servations and analyses at single river basins and comparisons across several of them at
113 continental levels. In European river basins, for which long flow records and historical
114 water coverage data are available, short flooding episodes (lasting hours to days) have
115 been linked to precipitation of differing duration as well as snow/thaw episodes (e.g., Blöschl,
116 2022; Hall & Blöschl, 2018; R. Merz & Blöschl, 2003) and revealed strong interactions
117 with antecedent conditions, e.g., soil moisture (Bertola et al., 2021; Blöschl et al., 2017)
118 (see also Wasko et al., 2020b; Tramblay et al., 2021, for soil moisture relevance in south-
119 eastern Australia and Africa, respectively). At the continental level in Europe, complex
120 shifts in flood timing patterns in response to climate change have been documented, in-
121 cluding seasonal anticipations in the snowmelt-driven Northeast, delays in storm-led floods
122 around the Mediterranean and North Sea, as well as overall reductions in the South and
123 East and rises the Northwest (Parajka et al., 2010; Blöschl et al., 2017, 2019; Bertola et

124 al., 2021). In North America this was also manifested, as a shortage of the snow accu-
 125 mulating season and consequential earlier onset of thaw and lower spring flood magni-
 126 tudes have been evidenced for the last thirty years (from weather and gauging stations;
 127 Burn & Whitfield, 2016; Cunderlik & Ouarda, 2009; Stewart et al., 2005; Wasko et al.,
 128 2020b) (but see also Villarini, 2016). In the flatter tropical setting of the Amazon basin,
 129 where floods display slower seasonal timings as explored through remotely sensed infor-
 130 mation and streamflow records, the effects of rainfall on flooding are strongly mediated
 131 by regional water table dynamics (Miguez-Macho & Fan, 2012; Papa et al., 2013). Un-
 132 der drier and (even) flatter settings in Argentina, flood pulses are not linked to well-defined
 133 river basins but are associated instead with the expansion and coalescence of isolated
 134 surface water bodies connected with rising water table levels (Aragón et al., 2011; Kup-
 135 pel et al., 2015). Floods in these regions, as well as in southeastern Australia, have shown
 136 multiyear fluctuations and have evidenced a high sensitivity to the interactive effects of
 137 climate fluctuations and land cover changes across the last thirty years (Tulbure & Broich,
 138 2019; Viglizzo et al., 2011; Whitworth et al., 2012).

139 When considering the global drivers of flooding at large spatial and temporal scales,
 140 it is also important to recognize the overwhelming role of topography over climate driv-
 141 ing groundwater depth at the planetary level (Fan et al., 2013). When we increase the
 142 observation scale, saturation may progressively gain dominance over infiltration as the
 143 flood-generating process (Blöschl, 2022), likely favored by regional topography and shal-
 144 lower water tables (Anyah et al., 2008; Jencso & McGlynn, 2011; Jobbágy et al., 2017).
 145 This possible connection between large-scale, slow flooding and topography and its in-
 146 terplay with climate has not been empirically and quantitatively assessed to our knowl-
 147 edge. In this sense, hydrologically-conditioned topography (hereby hydro-topography),
 148 based on the average water table depth and associated with the probability of conver-
 149 gence and stagnation of surface water, is one useful parameter to explore the sensitiv-
 150 ity of flooding to the most relevant effects of topography.

151 Here we narrow the definition of timing as the dominating timescale of flood fluc-
 152 tuations (e.g., seasons, years, decades) to evaluate their differing sensitivity to regional
 153 drivers. Focusing on slow floods captured by monthly-revisiting sensors onboard satel-
 154 lite platforms (e.g., Landsat), we hypothesize that (1) climate drives the timing of floods
 155 through their climatological average rainfall and temperature regimes (e.g., from hot arid
 156 to cold humid), (2) topography drives the extent of floods at a regional level, facilitat-
 157 ing saturation as the regional average water table level nears the surface, and (3) that
 158 the way in which both drivers combine at a given location is a result of their interplay
 159 mediated by geographical attributes, especially their latitudinal distribution. As shown,
 160 remote sensing provides a unique opportunity to study floods in a consistent way, cov-
 161 ering the whole climatic and topographic combination set, and with records going as far
 162 back as 1985 for monthly, 30-meter pixels (Pekel et al., 2016a; Pickens et al., 2020). By
 163 looking at how floods distribute globally in time and space, by exploring patterns in their
 164 timings' similarity, and by comparing their traits across all possible combinations of to-
 165 pography and climate we might be able to provide evidence on how geography controls,
 166 offsets, or even intensifies the influence of regional drivers on flood temporal dynamics.

167 2 Data and methods

168 2.1 Data selection

169 To conduct this large-scale study we used Google Earth Engine, an online open pro-
 170 cessing platform that holds an abundant data catalog of continuous update and provides
 171 high-performance cloud computing, allowing researchers to process large amounts of data
 172 in next-to-negligible times (Gorelick et al., 2017; Kumar & Mutanga, 2018). Flood ex-
 173 tent was estimated through the monthly, 30-meter resolution Global Surface Water Ex-
 174 tent dataset v1.3 (GSWE, Pekel et al., 2016a), which is available in Google Earth En-

175 gine for the period between 1985-2020. We limited our analysis to 1990-2020 to have three
 176 full decades of data, excluding the beginning of the Landsat missions for which there is
 177 a limited imagery distribution. Meteorological information (i.e., precipitation and tem-
 178 perature) was derived from TerraClimate, a monthly, 0.04° (~ 5 km at the Equator) grid-
 179 ded dataset available for the 1958-2021 period (Abatzoglou et al., 2018a). Climatic char-
 180 acterization was based on Köppen-Geiger’s dominant climate types (Kottek et al., 2006b;
 181 Rubel et al., 2017). Topographic characterization was based on the discrete classifica-
 182 tion by Roebroek et al. (2020), where they integrate the complex effects of local and re-
 183 gional topography on hydrology (therefore, hydro-topography) based on modelled mean
 184 water table depth (as per Fan et al., 2013).

185 To characterize regional slow floods at a global level, we summarized their cover-
 186 age in a 1-degree rectangular grid, which is an appropriate spatial level to look into re-
 187 gional hydrological processes (covering extensions of hundreds of thousands square km,
 188 Blöschl & Sivapalan, 1995), while also matching other relevant remote sensing datasets
 189 (e.g., GRACE, Tapley et al., 2004, 2019). We started off with 12,500 cells that exclu-
 190 sively covered continental terrestrial surface, excluding Antarctica. The monthly-level
 191 data was pre-processed and aggregated by cell in Google Earth Engine, and extracted
 192 to an R environment for further filtering, completion of analyses and plotting (see Data
 193 Availability Statement).

194 **2.2 Data filtering and hydrologic year reconstruction**

195 First, we filtered the GSWE dataset according to surface water variation in each
 196 30x30 m pixel between 1990 and 2020. Within the Google Earth Engine platform, and
 197 prior to cell-level aggregation, we masked those 30-meter pixels with a coefficient of vari-
 198 ation lower than 30%. This threshold proved to satisfactorily exclude lakes and other
 199 permanent water bodies across diverse regions (Figure 1). We then aggregated the monthly
 200 flooded fraction per 1°x1° cell (i.e., flooded extent) and obtained the regional time se-
 201 ries, to which we applied a two-step decision filter to have the best flood-representing
 202 time series while acknowledging frequent cloud-induced data gaps. To that end, we (i)
 203 excluded months with less than 75% of valid observations, and (ii) excluded cells that
 204 had less than 40% qualifiable months over the analyzed period (mainly due to cloud cover).
 205 Afterwards, we obtained the month where the flooded extent was at its minimum for each
 206 calendar year. The median value across all years was thus set as the start of the hydro-
 207 logic year. While this is accurate in unimodal surface water dynamics, for bimodal or
 208 non-modal (non-uniform) series (see Data Availability Statement) we took the first month
 209 that was returned. We also extracted the maxima (peak-occurring months) to associate
 210 floods with two main triggers, precipitation and snowmelt.

211 **2.3 Surface water variability and its decomposition**

212 We classified all cells according to the apportionment of temporal variability to (i)
 213 seasonal and (ii) interannual fluctuations, and (iii) long-term changes (i.e., net gain or
 214 loss over at least 20 years) through a K-means-based, conceptual decision tree. We also
 215 sought to further divide the seasonally dominated cells, considering two sub classes based
 216 on their association with rainfall and snowmelt, and the long-term class reflecting the
 217 direction of change (positive or negative). As a result, we obtained six classes (Figure
 218 S1), which summarize the dominant timescale at which flooding fluctuates (e.g, season-
 219 level, year-level or decade-level). The equations for the decomposition are explained in
 220 this section and exemplified in Figure 2.

221 After applying quality filters to the monthly time series of 1-degree flood extent,
 222 we described each cell through mean, maximum, and minimum extent descriptors, and
 223 through two measures of variability: variance (σ^2) and coefficient of variation (CV). Be-
 224 cause the temporal data was incomplete, often with large gaps of information, we de-

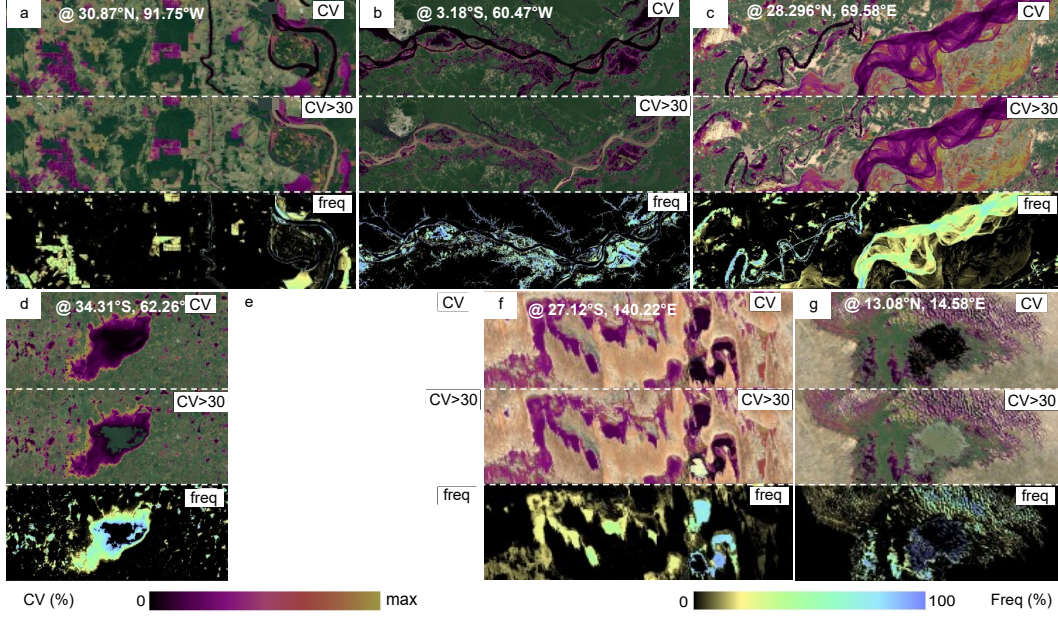


Figure 1. Examples of surface water masking result according to the coefficient of variation of each pixel (threshold = 30%), showing coefficient of variation (top panel), coefficient of variation after masking (central panel) and water cover frequency (bottom panel). (a) Mississippi River, United States; (b) Amazon River, Brazil; (c) Indus River, Pakistan; (d) Picasa Lake, Argentina; (e) glacial lakes in Russia; (f) Coongie Lakes, Australia; (g) Lake Chad, Chad.

225 cided to apply a simple decomposition based on segmented averages to characterize the
 226 variance instead of other approaches (e.g., BFAST; Verbesselt et al., 2010) that require
 227 gap-filled time series.

228 First, we propose that the temporal function of flooded extent (FE) is defined by
 229 a combination of cycles or timescales of differing duration, therefore:

$$230 \quad FE_t = T_t + IA_t + ST_t + r \quad (1)$$

231 where T_t is the long-term or trend component, which describes a net loss or gain
 232 of FE ; IA_t is the interannual component that points to year-to-year variations (akin to
 233 deseasonalization methods); ST_t is the seasonal component, describing the degree of sea-
 234 sonal fixation (wet season/dry season); and a final error component (r). The function's
 235 variance is an additive combination of the variances of each component:

$$236 \quad \sigma^2_{FE} = \sigma^2_T + \sigma^2_{IA} + \sigma^2_{ST} + \sigma^2_r \quad (2)$$

237 To quantify the apportionment of each component (*compweight*), we isolated them
 238 and calculated a coefficient of determination, i.e., the fraction of the variance that is ex-
 239 plained by them, through:

$$240 \quad comp\ weight_{\%} = \frac{\sigma^2_{comp}}{\sigma^2_{FE}} * 100 \quad (3)$$

We explored long-term trends of flood extent through a Mann-Kendall test. If the test was significant ($p < 0.001$), a trend slope was derived using the Theil-Sen slope estimator (Sen, 1968; Theil, 1992), which is a common methodology employed in the exploration of trends in hydrology (e.g., Wasko et al., 2020a; Kemter et al., 2023; Blöschl et al., 2017). Then, a long-term series was simulated from the resulting slope coefficient, and its variance was calculated and compared against the FE variance following Eq. (3). It is important to note that long-term trends were only explored in landscapes with at least 20 years of high-quality data, as trends found over shorter periods (e.g., 10 years) might be the result of fluctuations at the year level. Figure S2 locates the “blind spots”, i.e., landscapes that did not suffice the minimum timeseries extent according to the filters described in Section 2.2.

The interannual component (IA) corresponds to the effect of hydrologic-yearly means, following the function:

$$IA_t = \begin{cases} FE_y & \text{if } T = 0 \\ FE_y - T & \text{if } T \neq 0 \end{cases} \quad (4)$$

where FE_y is the flooded extent averaged for the y th hydrologic year (as defined in the previous section). It should be noted that, if the series had a trend component, part of the interannual component (IA) is explained by the long-term trend. Thus, when a trend was found, the interannual component was calculated as $IA - T$.

We define seasonality as the dynamic that reveals a fix wet and dry season. Even though temporary accumulation of water leads to seasonal floods (i.e., non-permanent), we were further interested in describing how fixed those peaks were. We thus defined seasonality (ST) as the function given by:

$$ST_t = FE_m \quad (5)$$

where FE_m is the flooded extent averaged for the m th month.

The error term may be thought of as the fraction of variance that cannot be explained by a single component (i.e., residual variance). This could be due to erratic, non-cyclic fluctuations (at the described timescales) or due to a combination of components that, by themselves, contribute to a small part of the fluctuations (i.e., codominance).

We classified flood timings firstly according to the dominant aspect of its temporal variability through a K-means (Hartigan & Wong, 1979) clustering of four centers, with 500 random initial sets and 1000 iterations. The means of the clusters were interpreted to label each class, and the long-term class was further divided in positive- and negative long-term trend depending on the direction of the LT slope (Figure S1).

2.3.1 Two drivers of seasonality

Seasonal floods can directly result from seasonal precipitation regimes, in which case lags are expected to be short and related to concentration and accumulation times. Yet, they can also be mediated by sub-zero temperatures dictating freezing and thaw cycles, and leading to longer lags and decoupling from precipitation seasonality. We analyzed the temporal proximity of flooding peaks to precipitation peaks as well as to the endings of sub-zero temperature period for all the cells in which the seasonal component was dominant. For this purpose, we calculated lags between precipitation and flooding peaks for each cell and performed bootstrapped simple linear regression, which iterates over thousands of samples resulting from permutations with replacement of the population, to extract the median intercept and slope of peak-to-peak lag relationship. We

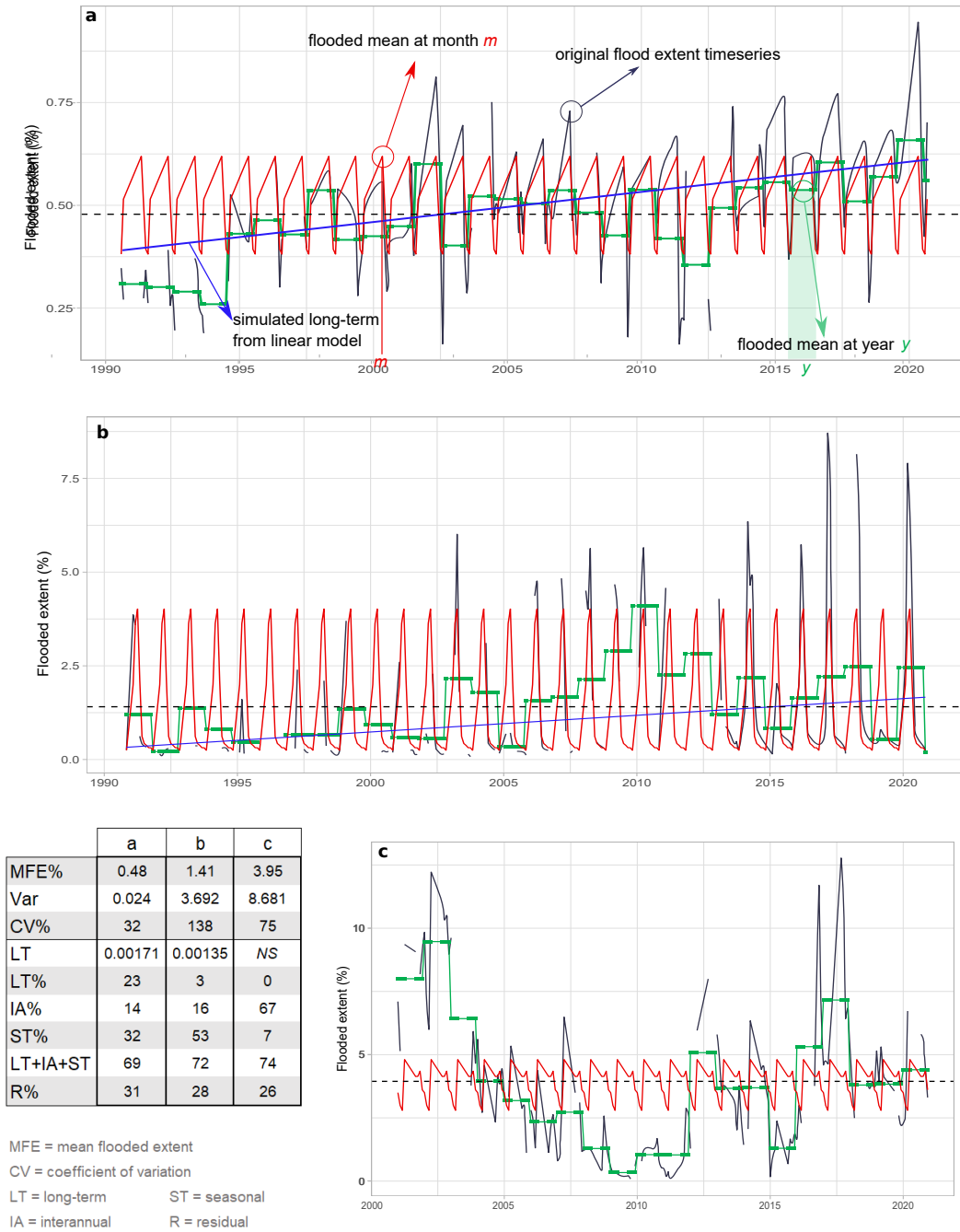


Figure 2. Example of timeseries segmentation into long-term (LT, blue line), interannual (IA, green line) and seasonal (ST, red line) components, with the remaining variance being considered “residual” (R, calculated as 100 minus the sum of LT, IA, and ST relative contributions to the total variance) for three cells: (a) one where there is seasonal and interannual codominance (centered at 52.5°N, 92.5°W), (b) one where seasonality dominates (centered at 15.5°S, 23.5°E), and (c) one where interannual fluctuations dominate (centered at 35.5°S, 62.5°W). The dashed line represents the overall mean flooded extent (MFE).

also included local regression analyses (i.e., LOESS) which generate smoothed regressions along the data, allowing to interpret visually the form of the relationship between the landscape’s precipitation and flooding peaks (see Section 2.2). In order to distinguish whether seasonality was driven by rainfall or snowmelt we assumed that a landscape cell had snowmelt effects when it had (a) at least two consecutive months of sub-zero mean temperatures, and (b) a lag of at least four months between precipitation peak and flooding peak. Landscapes that did not follow both criteria were assumed as being directly associated to rainfall. This approach discerned regions with sub-zero winters whose precipitation peaks escape freezing-thawing effects and are closely coupled with floods from those where seasonal flooding cycles are clearly controlled by temperature.

2.4 Flood dynamics across climate and hydro-topography gradients

Last of all, we explored how the observed flooding attributes are associated with climate and to hydro-topography (see Section 2.1). The five climate classes used (A – equatorial, B – arid, C – warm temperate, D – snow/boreal, E – polar) capture the likelihood of water excess generation and of its temporary retention as ice, while the seven classes of hydro-topography (1 – open water and wetland, 2 – lowland, 3 – undulating, 4 – hilly, 5 – low mountainous, 6 – mountainous, 7 – high mountainous) capture a gradient that ranges from high convergence and stagnation to high divergence and drainage that integrate some of the most relevant effects of topography on flooding. We summarized each attribute through a majority value per landscape cell (Figure S3).

3 Results

3.1 Flooding descriptors

Flooded areas display a highly skewed geographical distribution (Figure 3). The mean flooded extent (MFE) of all grid cells averaged 0.48% across all continents excluding Antarctica, with 73.4% of the total flooded area concentrated in the top 20% most flooded grid cells (Figure S4). Slow (long-lasting) floods showed a dominant latitudinal gradient, where northern Eurasia and North America hold the largest share of highly water-covered cells (MFE > 10%) (Figure 3 a). Outside the boreal belt, the valleys of some of the largest rivers and important wetland areas in Africa (Nile, Congo, Niger, and Zambezi rivers), Asia (Ob, Taz, Lena, Indus, Brahmaputra, Ganges, and Yangtze rivers, Poyang Lake), and South America (Amazon, Beni, Paraná, Orinoco and Ucayali rivers, Iberá and Orinoco Llanos wetlands) contributed the next largest number of highly flooded cells.

The overall temporal variability of floods, as captured by the coefficient of variation, revealed a general stable water coverage (CV < 50%, 56.3% of cells) in areas with most flooded area coverage (MFE > 1%) (Figure 3b, S5a), particularly across North America, Amazonia, Europe, and northeastern Asia. Moderate temporal variability (50 < CV < 200 %, 32.5% of cells) took place in all continents and its highest fraction was aggregated in central and southern Argentina, the Sahel and Okavango regions in Africa, central Asia, eastern China, and all across Australia. Lastly, extreme variability (CV > 200%, 11.2% of cells) was found in western and central Australia, northern Sahel, the Saharan desert, the Arabian Peninsula, and Iran.

The decomposition of the variance of flood extent through time showed that seasonal, interannual, and long-term components explained together, on average, 68% of the total variance (more than 90% in the top decile and less than 43% in the lowest decile). Particularly remarkable is the fact that seasonality dominated the variance of 34.1% of the cells, followed by interannual fluctuations (18%) and long-term changes (11.1%). In the rest of the cells (36.7%) more than one timescale of variance prevailed (i.e., interannual and seasonal codominance). The geographic control was evident in the seasonal-to-interannual dominance shift with a distinctive threshold at the -20° latitude (Figure

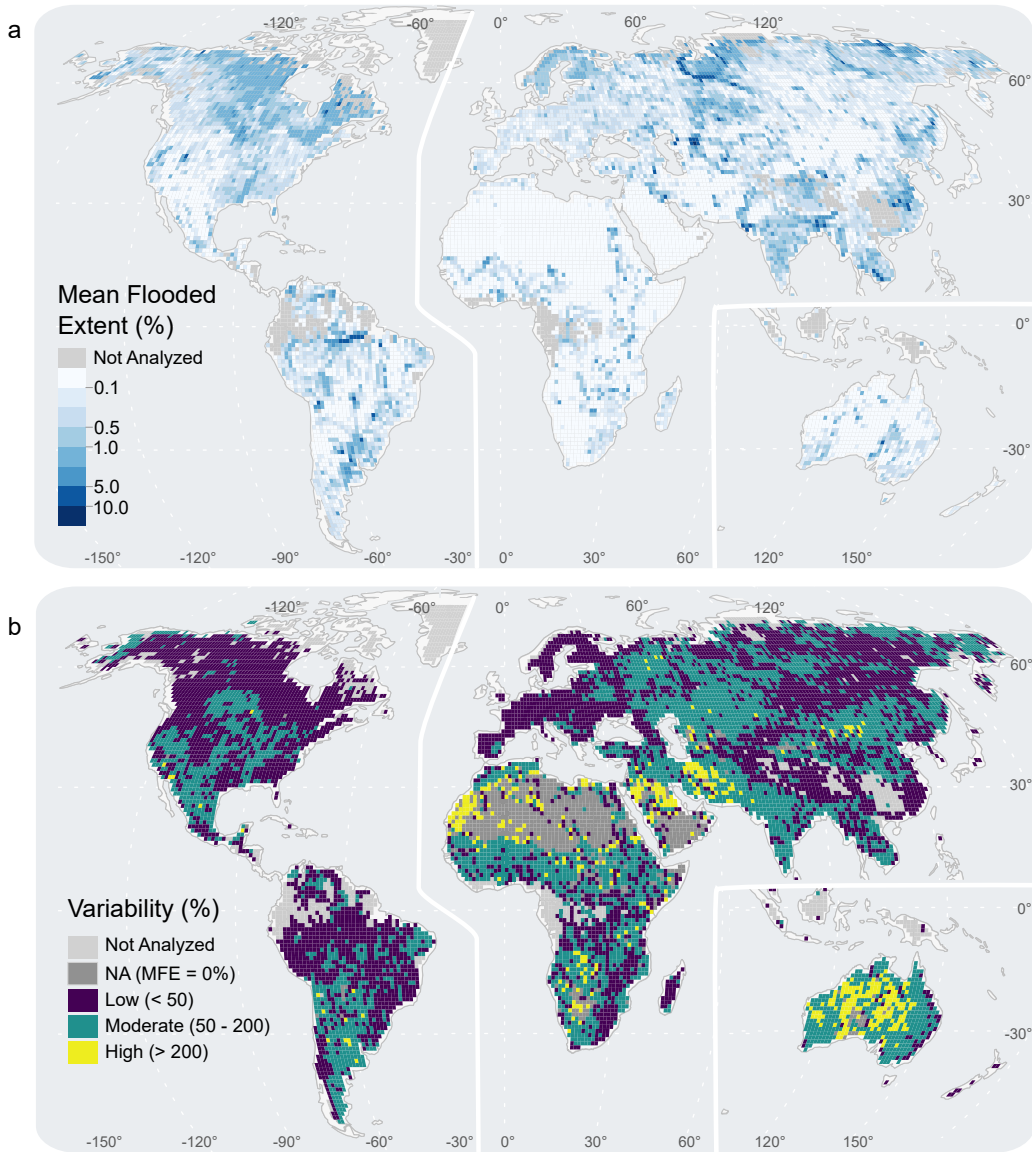


Figure 3. Global distribution of flooding extent (a, mean monthly values) and temporal variability of landscapes with mean flooded extent greater than 0% (b, coefficient of variation). Note that the color scales are nonlinear

334 4 and Figure S5b). Seasonality dominated flood timings across the northern hemisphere
 335 and the tropics, while interannual flooding fluctuations were dominant in northeastern
 336 Brazil, Argentina, South Africa, and eastern Australia. Over the United States, a transi-
 337 tion from seasonal to interannual dominated flooding fluctuations coincided with the
 338 aridity gradient that has its most conspicuous limit along the -97° meridian (Figure S6).

339 Long-term change (i.e., net gain or loss of flooded area) dominated flooding vari-
 340 ability in 11.1% of the cells, with positive trends outweighing negative ones (9.85 and
 341 1.25%, respectively). Positive long-term trends were distributed across all latitudes and
 342 were especially important in Europe and central Asia, with magnitudes of up to 1300
 343 km^2 of net flood gain. In contrast, negative long-term trends, which dominated 1.2% of
 344 flood timings, were mainly found in mid-latitudinal regions (Figure S5c). Positive long-

345 term dominated dynamics were not as spread nor aggregated as seasonal- and interannual-
 346 driven fluctuations, except in China and Canada. Negative change appeared mostly in
 347 the Aral Sea, southern Argentina, and central United States (Figure 4, S5c) and may
 348 reflect well-documented patterns of increased droughts and irrigation impacts.

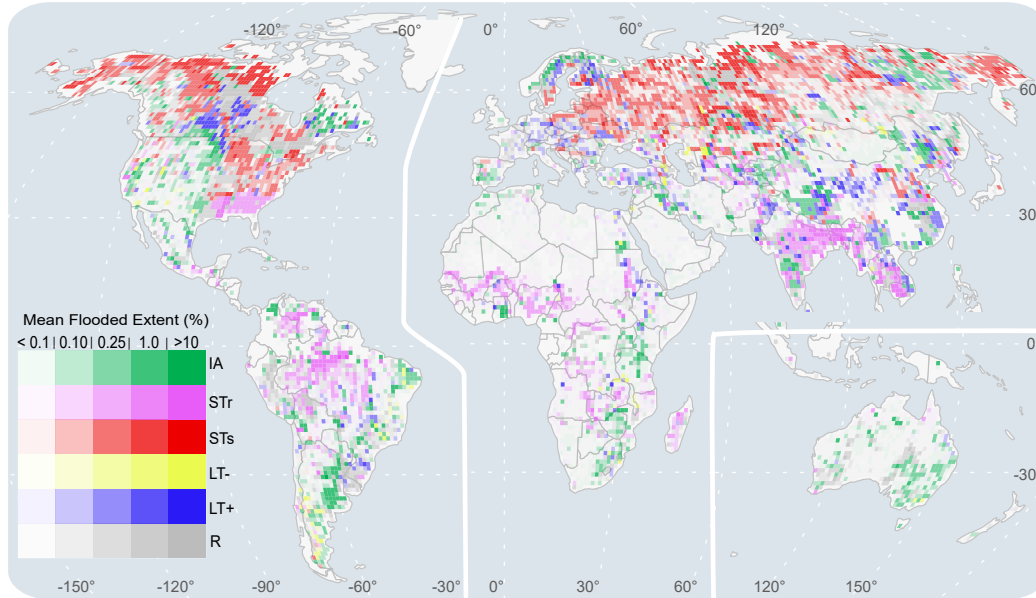


Figure 4. Classification of flood timings according to the major pattern of temporal fluctuation (or lack thereof): interannual (*IA*, green), rainfall-driven seasonal (*ST_r*, magenta), snowmelt-driven seasonal (*ST_s*, red), negative long-term trend (*LT₋*, yellow), positive long-term trend (*LT₊*, blue), and residual (*R*, gray). Color intensity reflects Mean Flooded Extent in a nonlinear scale. It should be noted that a cell might be subject to contributions from more than one timing component (e.g. seasonal with long-term trend), yet the dominant one is highlighted.

3.2 Flooding attributes across climatic and hydro-topographic gradients

349

350 Flooding descriptors responded differently to climate and hydro-topography (Figure
 351 5). The magnitude of flooding (as captured by MFE) was mainly explained by hydro-
 352 topography, being exponentially biased towards the flattest positions (type 1, open water
 353 and wetland, and type 2, lowlands, both characterized by extremely shallow water
 354 tables, Figure S3) which had four times more water covered area than the rest of the land-
 355 scapes, hosting 12% of the flooded areas in just 4.54% of the global land (Figure 5 and
 356 Table S1). Outside these hydrologically stagnant cells, undulating to hilly landscapes (types
 357 3 and 4) held 78.17% of global flooded area with a share of 75.88% of global land. These
 358 figures dropped for mountainous cells (types 5-7) which hold 9.82% of global flooded area
 359 hosting 18.92% of the global land. Climate appeared as a subordinate factor but no less
 360 crucial, showing how the Boreal type held the largest share of floods (40% of global flooded
 361 area in 24.77% of the global land) and, together with Equatorial type, had more than
 362 twice and three times more average flooding than Arid and Temperate types (Figure 5
 363 and Table S1).

364

365 Total temporal variability (which had a global average coefficient of variation of
 366 68.4%) peaked towards flat arid landscapes (mean CV = 141%) and decreased towards
 367 both more complex and flatter landscapes (Figure 5c). Results showed that hilly and moun-

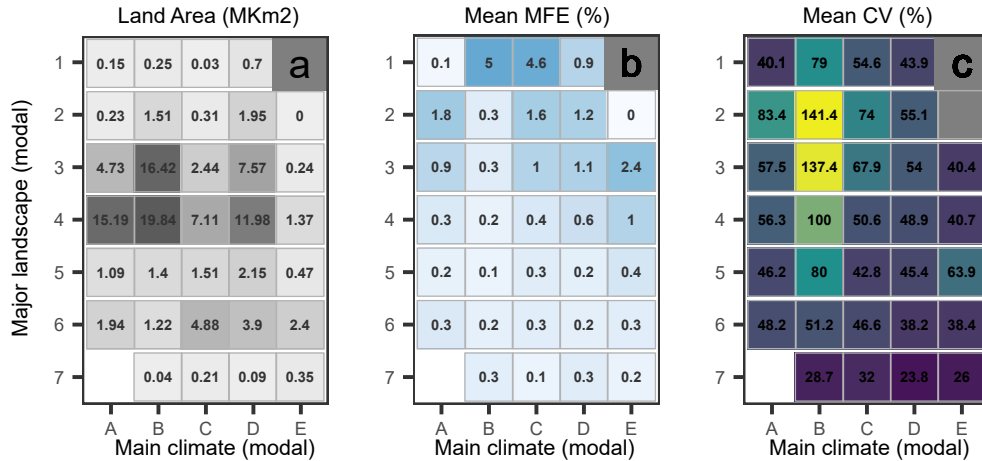


Figure 5. Allocation of flooding temporal descriptors regarding modal main climate (A – equatorial; B – arid; C – warm temperate; D – snow/boreal; E – polar) and modal hydro-topography position (1 – open water and wetland; 2 – lowland; 3 – undulating; 4 – hilly; 5 – low mountainous; 6 – mountainous; 7 – high mountainous). For all 12,500 continental cells (a) total land area (in Mkm²) per combination, and for the 11,443 analyzed cells: (b) mean MFE (%); (c) mean variability (%). Color scales in panels b-c are reproduced from those in Figure 3 a-b, respectively, which are nonlinear.

tainous cells with low mean water coverage had the most stable floods (mountainous and high mountainous mean CV = 42%). Total variability responded more clearly to climate, being lowest in the Polar climate type (mean CV = 42%) and highest in the Arid type (mean CV = 113%).

As temporal variability was segmented into seasonal, interannual, and long-term components some noticeable patterns emerged (Figure 6). The seasonal component dominated under both Equatorial and Polar climates and gradually yielded its dominance to the interannual component along the Boreal-Temperate-Arid gradient. Interannual variability was prevalent in intermediate hydro-topographies, especially under the Arid and Temperate climates. The positive long-term component of flooding temporal variability was most important in Polar regions, while the negative ones prevailed in Arid regions. Positive trends (most common in mountainous hydro-topographies under all climates) were more widespread than negative ones (most common in flat hydro-topographies with Arid climate).

3.3 Drivers of seasonal flooding

Seasonal fluctuations in flooding may respond to high/low precipitation and/or snow/thaw seasonal cycles, as suggested by the temporal (mis)match between flooding and precipitation peaks throughout the year under different climate types (Figure 7). Varying degrees of synchrony with rainfall seasonality evidenced temperature-mediated lags for flooding growing towards boreal regions after two types of regression analyses. Equatorial and Arid regions revealed the most immediate response of floods to rainfall timing, with a mean lag of 3.5 months, whereas Boreal territories adjusted better instead to the beginning of above-zero temperatures, showing a mean lag of 9.4 months.

Warm regions (climates A, B, and C) had the tightest synchrony between rainfall and flood, with a mean lag of 3.4, 3.7, and 5.2 months, respectively (Figure 7a and c).

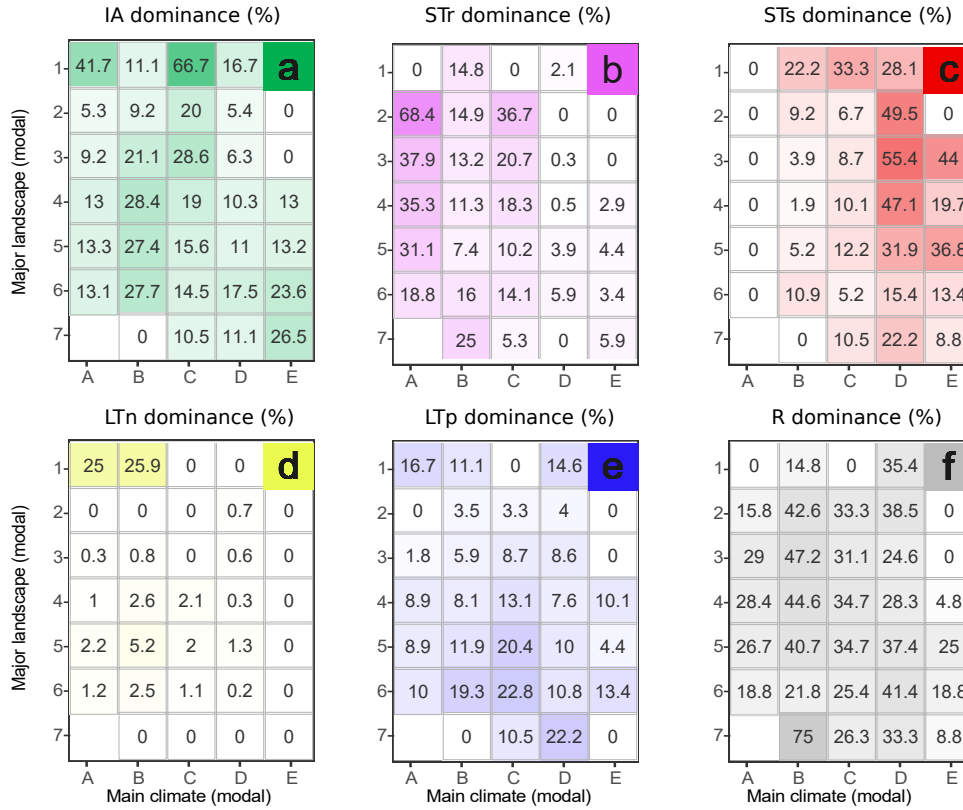


Figure 6. Allocation of flooding temporal descriptors regarding modal main climate (A – equatorial, B – arid, C – warm temperate, D – snow/boreal, E – polar) and modal hydro-topography position (1 – open water and wetland, 2 – lowland, 3 – undulating, 4 – hilly, 5 – low mountainous, 6 – mountainous, 7 – high mountainous). Percentage of cells dominated by (a) interannual, (b) rainfall-driven seasonal, (c) snowmelt-driven seasonal, (d) negative long-term trend, (e) positive long-term trend, (f) residual variance.

392 Bootstrapped linear regression sustained this association, showing how flooding peak tim-
 393 ing was greatly explained by precipitation peak timing for Equatorial climates (inter-
 394 cept = 3.2, slope = 1.05, $R^2 = 0.83$), while rainfall-driven cells of Arid and Temperate
 395 climates presented similar coefficients (intercept = 2.7 and 2.83, slope = 0.98 and 1.07,
 396 $R^2 = 0.58$ and 0.7, respectively; Figure S7). Local regression analyses (through a LOESS
 397 smoothing function, Figure S8) showed how, for Arid and Temperate climates, an increase
 398 of flood-lag in cells where precipitation would peak between May and September while
 399 floods peaked between March and May, hinting a decoupled flooding pattern. These were
 400 all distributed north of the 30° latitude, where monthly minimum temperatures drop be-
 401 low 0°C in the cold season and could disassociate floods from precipitation (to an up to
 402 10-month lag) independently of the cell’s proportion of snow inputs.

403 In contrast, in the vast fraction of the northern hemisphere registering subzero winter
 404 temperatures (climates D and E), seasonal floods occurred mainly where snow pre-
 405 cipitation inputs were highest (snow fraction > 30%) and were initiated by the onset of
 406 snowmelt between April and June of the following calendar year (Figure 7b, circles). This
 407 translates into an up to one month lag to minimum temperature rise above 0°C, and into
 408 a great dissociation from precipitation peak (between 8 and 10 months, Figure 7d and
 409 S7). Some Polar- and Boreal-dominated cells showed floods closer to precipitation peaks

410 when they occurred earlier in the calendar year. Regression analyses based on bootstrapped
 411 linear models reflected this association (intercept = 0.45 and 1.01, $R^2 = 0.74$ and 0.92,
 412 respectively; Figure S7). In these cases, we found that either snow inputs were minor (snow
 413 fraction < 30%) and/or that precipitation coupled with the initiation of above-zero tem-
 414 peratures, so the effect of temperature mediating in the translation of rainfall to flood
 415 was not as prevalent (Figure 7b and d, triangles).

416 4 Discussion

417 Here we present a novel, global characterization of the timing of slow floods. By
 418 segmenting monthly time series into short, intermediate, and long timescales of fluctu-
 419 ation we were able to identify and map regions with similar flood timing. Based on this
 420 geographic characterization of water coverage patterns we provide evidence about the

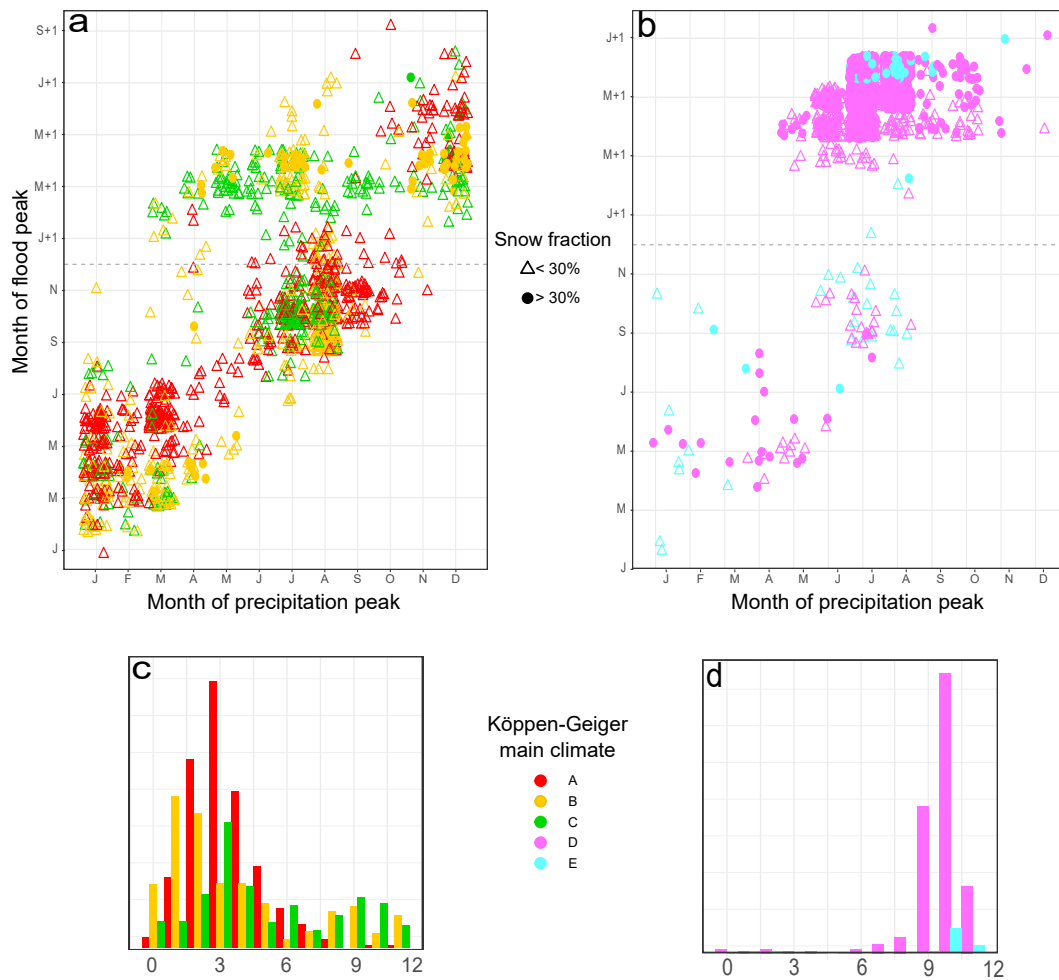


Figure 7. Seasonality of precipitation and floods. Month of flood peak vs. month of precipitation peak for (a) Equatorial (red), warm Temperate (green) and Arid (yellow), and (b) Boreal (purple) and Polar (light blue) Köppen-Geiger climate (KG) dominated cells, differentiating conditions of low (empty triangles) and high snow inputs (circles). Where floods peak on the following calendar year in respect to precipitation, “+1” is indicated. Jitter does not suggest exact dates but is used for a better display of the data. Subplots c) and d) show the precipitation-to-flood peak lag distribution, in months, for each climate type.

421 large-scale drivers of flooding dynamics, thanks to the exploration of flood attributes across
422 the wide range that regional climate and topography achieve at the global scale. In the
423 first place, we propose how this new geographical perspective of flood timing can aid dif-
424 ferent global hydrology research avenues. We then focus on the main lessons that it of-
425 fers about the roles of topography and climate and their interactions driving flooding
426 dynamics. Lastly, we show how these geographical findings provide insight into the dif-
427 fering sensitivities of flooding to global change.

428 Setting floods in a geographical context allows for exploring patterns influenced by
429 broad environmental gradients including wide latitudinal effects. The distribution of global
430 flood timings, based on the predominant timescale of their fluctuations, revealed that
431 while many highly flooded regions of the world have a predictable flood seasonality, an-
432 other large fraction experiences floods whose major fluctuations span multiple years. In
433 fact, seasonality dominates flood timing across the boreal and tropical belts, yielding to
434 predominantly interannual timing-dominated fluctuations south of the -20° latitude (Fig-
435 ure 4 and S5). This distinct hemispheric effect could be explained by a lower temper-
436 ature and precipitation seasonality (i.e. more oceanic climate of the austral temperate
437 belt) which may be overridden by multiyear sources of fluctuations such as ENSO (Kundzewicz
438 et al., 2019; Silva et al., 2017). One important implication of these patterns is that for
439 at least one-fifth of the terrestrial surface, flood analyses should encompass several years
440 to capture the typical span of flooding conditions.

441 We envision that an explicit global geography of floods, one for which the cartog-
442 raphy generated in this study (Figures 3 and 4) is an initial contribution, has two ma-
443 jor applications for hydrology research. On one side, it serves as a guide for the synthe-
444 sis and extrapolation of local studies on flood causes, dynamics, and consequences across
445 regions with similar flood timings. On the other side, it can help select the most appro-
446 priate assimilation strategies for land surface models incorporating the currently over-
447 looked effect of flooding on water and energy fluxes, by showing where floods must be
448 accounted for and at what temporal scale their variability should be represented. Sev-
449 eral studies have shown how coupling global climate models with land surface models
450 that incorporate surface water dynamics substantially improves the estimation of energy
451 and greenhouse gas fluxes (e.g., Schrapffer et al., 2020; Getirana et al., 2021) as they are
452 key in the energy feedback between the surface and the atmosphere (Houspanossian et
453 al., 2018; Krinner, 2003).

454 The drivers and process explaining a phenomenon under study depend on the ob-
455 servation scale (O’Neill et al., 1986; Blöschl & Sivapalan, 1995). We conducted our study
456 at a large scale and explored how flood attributes (i.e., mean extent, variability, and tim-
457 ing) respond to regional climatic and topographic constraining drivers. Our analysis demon-
458 strated how high levels of water convergence and groundwater proximity to the surface
459 resulting from regional topography were the main control of surface water accumulation,
460 even after excluding large water reservoirs of low variability (pixels varying less than 30%
461 of the observed period). Landscapes with regional water tables closer than 0.25m (hydro-
462 topographic class 1, mean flooded extent = 1.77%) were two to four times more likely
463 to flood than undulating to hilly regions (mean flooded extent = 0.38 to 0.98%), and ten
464 times more likely to flood than mountains (mean flooded extent = 0.19 to 0.23%) (Fig-
465 ure 5). Fan et al. (2013) estimated that at least 15% of the continental surface water may
466 be in contact with shallow water tables, while several local studies have illustrated the
467 sensitivity of the groundwater-surface contact in that portion of the world to land use
468 and vegetation changes (Cramer & Hobbs, 2002; Favreau et al., 2009; Giménez et al.,
469 2020; Ibrakhimov et al., 2018). Whether the regional mechanism explaining the link be-
470 tween topography, water table, and flooding is dominated by saturation or infiltration
471 processes (Blöschl, 2022) is an attractive question to follow this analysis. For instance,
472 it could be addressed by looking into the shape of the evolving relationship between rain-

473 fall, runoff, water table levels and flooded extent (e.g., Gelmini et al., 2022; Reager et
474 al., 2014; Zuecco et al., 2016) at a regional level.

475 Climate was more important than topography in explaining the temporal variability
476 of floods and their timing. Predictable, seasonally-dominated fluctuations in cold re-
477 gions gave place to interannual and mixed patterns in temperate climates, and to more
478 irregular and unpredictable patterns in arid regions (Figures 5 and 6). The link between
479 climate, flood peak seasonality, and flood-generating processes has been explored in the
480 contiguous United States (Saharia et al., 2017), where the subordinate climate (with vs.
481 without dry season), as well as the geographical context (inland vs. coastal and inter-
482 mountainous vs. flatland), also helped explain the varying magnitude of the represen-
483 tative peak discharge. We further identified the process triggering regionally seasonal
484 floods (i.e., rainfall vs. snowmelt), finding that freezing/thawing pulses dictated by tem-
485 perature seasonality rule flood timings in boreal climates (Figure 6). A third flood-generating
486 process that was included within the rainfall trigger is rain-on-snow events, which were
487 in this study located in northwestern United States, and central and eastern Asia, yet
488 can be locally relevant as demonstrated in Europe (R. Merz & Blöschl, 2003; Viglione
489 et al., 2016; B. Merz et al., 2021), United States (McCabe et al., 2007; Stein et al., 2020)
490 and more recently, over the northern polar belt (Cohen et al., 2015).

491 While our study did not attempt to attribute long-term trends to causal mecha-
492 nisms or to the effect of temporal changes in each driver (e.g., climate regime shifts or
493 large-scale topographic modifications), it helps hypothesize on the phenomena that may
494 explain their prevalence as the major source of flooding variability across 11% of the ter-
495 restrial surface (Figure 4). Some large clusters of long-term flooding variability domi-
496 nance with prevailing positive trends observed in Europe, central Asia, and northern North
497 America point towards the effects of global warming, as supported by regional field stud-
498 ies (B. Merz et al., 2021; Woldemeskel & Sharma, 2016) and modeling efforts (Meriö et
499 al., 2019; Vormoor et al., 2015); or the interactive effects of global warming and shift-
500 ing precipitation regimes (Bertola et al., 2021; Song et al., 2014; Viglione et al., 2016;
501 K. Yang et al., 2014; L. Yang et al., 2021). In other regions, land use may be the pre-
502 vailing driver, for instance in the cluster in north-eastern China, corresponding to the
503 Songnen plain, where paddy rice has expanded over native grasslands over the last thirty
504 years, likely increasing the amount and duration of water coverage (Liu et al., 2009; Wang
505 et al., 2009; Y. Zhang et al., 2019). In contrast, long-term negative trends in flooding
506 were less abundant and more fragmented. The conspicuous case of the Aral Sea, explained
507 mainly by the impacts of irrigation infrastructure (Jin et al., 2017; Micklin, 1988) ap-
508 pears to be accompanied by other situations in which irrigation may play an important
509 role such as the Mendoza-Colorado rivers in Argentina (Rojas et al., 2020).

510 Surprisingly, vast areas of increasing flooding detected in our study like that in south-
511 central Canada which may be a result of changes in climate interacting with agricultural
512 practice shifts (Hayashi et al., 2016; J. Huang et al., 2016; Wang & Vivoni, 2022), are
513 poorly explored in the literature. A noticeable aspect of this flood-gaining region is its
514 location in the transition from seasonal-dominated to interannual-dominated flood tim-
515 ings (Figure 4). We speculate that flooding shifts there could be associated with a regime
516 switch from a more regular temperature control to a more variable precipitation control
517 of flood timing (see Chegwiddden et al., 2020; Wang & Vivoni, 2022; S. Zhang et al., 2022).
518 In Patagonia, we detected a less-aggregated, negatively-trended cluster which is alarm-
519 ing given the increasing susceptibility to drying of lakes in semi-arid regions. There has
520 been recent evidence generated that indicates how the shallow Colhué Huapi Lake in cen-
521 tral Patagonia might be following the Aral Sea's fate, though it is unclear whether it is
522 related to snowpack depletion, increased extraction for human and livestock consump-
523 tion, decreased precipitation, or a combination of all (Carabajal & Boy, 2021; Scordo et
524 al., 2018). Thus, a key takeaway from our analysis is that a global framework can ac-

525 tually help connect research lines and generate hypotheses arising from the observed re-
526 gional patterns.

527 Lastly, we believe that a continuous update of the geography of floods, as flood datasets
528 expand, will become relevant as it could indicate where and how future flood timings may
529 change in response to the effects of climate change. Furthermore, because intensification
530 of the hydrological cycle giving place to higher interannual variability (Huntington, 2006)
531 could result in detrimental effects on water and food security, more attention should be
532 put into understanding the dynamics of interannual-dominated timings. Over the last
533 32 years, interannual fluctuations have been dominating floods mostly in the global south
534 (i.e., Argentina, Australia, South America, South Africa, and Botswana) but also across
535 the United States, southern India, and northeastern China. By continuously monitor-
536 ing the dominant timing of floods at a global level, we could anticipate timing shifts (e.g.,
537 seasonal to interannual), especially where they are most likely to occur, i.e., in the tem-
538 perate and dry climate boundaries.

539 5 Conclusions

540 Upscaling and extrapolating our growing body of plot- to basin-level knowledge about
541 the mechanisms, drivers, and impacts of flooding is still challenging. With an explicit
542 representation of the global geography of floods, for which this work is an initial contri-
543 bution, we can contribute top-down insight into the most salient cross-regional flooding
544 patterns and their likely large-scale drivers. The global distribution and timing of “slow”
545 floods (those lasting at least a few days, in opposition to “flash” floods lasting only hours)
546 captured over the last three decades revealed that flooding extent was strongly dictated
547 by regional topography and its effect on the proximity of the water table to the surface
548 (i.e. hydro-topography), with climate having a secondary role. Low regional areas of wa-
549 ter convergence were 2-4 times more likely to flood than flat to hilly regions and 10 times
550 more likely to flood than mountains. Across major climate types, floods were more ex-
551 tensive in landscapes having seasonal sub-zero temperatures than the rest combined, sug-
552 gesting how freezing/thaw cycles favor pulses of liquid water accumulation beyond any
553 other climatic control. The timing of floods (i.e., the dominant timescale at which flood-
554 ing fluctuates) was mainly driven by climate with seasonality peaking in both equato-
555 rial and polar climates and interannual variability rising along the boreal-temperate-arid
556 gradient, with a clear global North/South hemisphere contrast. The dominance of long-
557 term flooding trends prevailed mainly in the boreal belt ($>50^\circ$ latitude), where floods
558 are gradually increasing their coverage. Global patterns of positive and negative long-
559 term flooding trends suggest that anthropogenic climate change may influence flooding
560 where warming accentuates thawing cycles (increasing flooding), eliminates freezing (de-
561 creasing flooding), or intensifies interannual precipitation variability. Yet, climate change
562 may have its most salient effect on the timing of floods at all temporal levels from sea-
563 sonal to long-term. As not only water security but the multiple aspects of ecosystems
564 and societies linked to floods are likely to respond to shifting flooding dynamics, it be-
565 comes crucial to keep improving our monitoring strategies and our conceptual models
566 of flood controls. In this sense, this study is an example of how large-scale studies with
567 a uniform global coverage serve as a guide for the synthesis and extrapolation of local-
568 to-continental studies on flood causes, dynamics, and consequences across regions with
569 similar flood timings. The detection of patterns and further comparison of the pathways
570 of flood timing across the planet can give place to hypotheses and novel studies in re-
571 gions that may have gone unnoticed.

Open Research

Data Availability Statement

This study uses data from multiple sources, the majority being freely available in the Google Earth Engine data catalog (<https://developers.google.com/earth-engine/datasets>). Flood extent is based on the Global Surface Water Extent dataset v1.3 (Pekel et al., 2016b). Meteorological data (precipitation and temperature) is derived from TerraClimate (Abatzoglou et al., 2018b). Köppen Geiger climates were downloaded from <http://koeppen-geiger.vu-wien.ac.at/present.htm>, (Kottek et al., 2006a) and hydrologically-conditioned topography from <http://www.hydroshare.org/resource/38ac7dd90c7d4353bb492604981782f0> (Roebroek, 2020). All timeseries were extracted to an R environment (R Core Team, 2021a) for filtering and completion of analysis, and visualization of results, through the doParallel (Microsoft Corporation & Weston, 2020a), factoExtra (Kassambara & Mundt, 2020), foreach (Microsoft Corporation & Weston, 2020b), ggplot2 (Wickham, 2016), ggpubr (Kassambara, 2020), Kendall (McLeod, 2022), moments (Komsta & Novomestky, 2015), robslopes (Raymaekers, 2022), stats (R Core Team, 2021b), sf (Pebesma, 2018), and tidyr (Wickham, 2021) packages. The exploration of distribution uniformity and modes extraction of flooding and precipitation was carried through the LaplacesDemon R package (Statisticat & LLC., 2021).

The derived flood inundation extent dataset and meteorological data associated with this study, as well as the R codes used for processing, analyzing and plotting in this study can be found at <https://doi.org/10.5281/zenodo.7328786> (Torre Zaffaroni et al., 2022).

Acknowledgments

This work was funded by a doctoral scholarship from the National Scientific and Technical Research Council (CONICET) and by the GovernAgua project granted by the Inter American Institute for Global Change Research (IAI SGP-HW 056). The authors declare no conflicts of interest relevant to this study. We thank the three anonymous reviewers for their constructive comments and suggestions which have made our article more compelling. We extend our thanks to S. Aguiar, P. Baldassini, G. Camba Sans, H. Dieguez, and L. Staiano for their valuable comments throughout the stages of the analysis.

References

- Abatzoglou, J. T., Dobrowski, S. Z., Parks, S. A., & Hegewisch, K. C. (2018a). TerraClimate, a high-resolution global dataset of monthly climate and climatic water balance from 1958–2015. *Scientific Data*, 5(1), 170191. doi: 10.1038/sdata.2017.191
- Abatzoglou, J. T., Dobrowski, S. Z., Parks, S. A., & Hegewisch, K. C. (2018b). *Terraclimate: Monthly climate and climatic water balance for global terrestrial surfaces, university of idaho* [dataset]. Retrieved from https://developers.google.com/earth-engine/datasets/catalog/IDAHO_EPSCOR_TERRACLIMATE doi: 10.1038/sdata.2017.191
- Alborzi, A., Zhao, Y., Nazemi, A., Mirchi, A., Mallakpour, I., Moftakhari, H., ... AghaKouchak, A. (2022). The tale of three floods: From extreme events and cascades of highs to anthropogenic floods. *Weather and Climate Extremes*, 38, 100495. doi: 10.1016/j.wace.2022.100495
- Alsdorf, D. E., Rodríguez, E., & Lettenmaier, D. P. (2007). Measuring surface water from space. *Reviews of Geophysics*, 45(2). doi: 10.1029/2006RG000197
- Anyah, R. O., Weaver, C. P., Miguez-Macho, G., Fan, Y., & Robock, A. (2008). Incorporating water table dynamics in climate modeling: 3. Simulated ground-water influence on coupled land-atmosphere variability. *Journal of Geophysical Research Atmospheres*, 113(7). doi: 10.1029/2007JD009087

- 621 Aragón, R., Jobbágy, E. G., & Viglizzo, E. F. (2011). Surface and groundwater dy-
 622 namics in the sedimentary plains of the Western Pampas (Argentina). *Ecology-*
 623 *hydrology*, 4(3), 433–447. doi: 10.1002/eco.149
- 624 Arora, A., Pandey, M., Siddiqui, M. A., Hong, H., & Mishra, V. N. (2021). Spatial
 625 flood susceptibility prediction in Middle Ganga Plain: comparison of frequency
 626 ratio and Shannon’s entropy models. *Geocarto International*, 36(18), 2085–
 627 2116. doi: 10.1080/10106049.2019.1687594
- 628 Aufdenkampe, A. K., Mayorga, E., Raymond, P. A., Melack, J. M., Doney, S. C.,
 629 Alin, S. R., . . . Yoo, K. (2011). Riverine coupling of biogeochemical cycles
 630 between land, oceans, and atmosphere. *Frontiers in Ecology and the Environ-*
 631 *ment*, 9(1), 53–60. doi: 10.1890/100014
- 632 Bertola, M., Viglione, A., Vorogushyn, S., Lun, D., Merz, B., & Blöschl, G. (2021).
 633 Do small and large floods have the same drivers of change? A regional at-
 634 tribution analysis in Europe. *Hydrology and Earth System Sciences*, 25(3),
 635 1347–1364. doi: 10.5194/hess-25-1347-2021
- 636 Blöschl, G. (2006). Hydrologic synthesis: Across processes, places, and scales. *Water*
 637 *Resources Research*, 42(3). doi: 10.1029/2005WR004319
- 638 Blöschl, G. (2022). *Flood generation: Process patterns from the raindrop to the ocean*
 639 (Vol. 26) (No. 9). Copernicus GmbH. doi: 10.5194/hess-26-2469-2022
- 640 Blöschl, G., Hall, J., Parajka, J., Perdigão, R. A. P., Merz, B., Arheimer, B., . . .
 641 Živković, N. (2017). Changing climate shifts timing of European floods.
 642 *Science*, 357(6351), 588–590. doi: 10.1126/science.aan2506
- 643 Blöschl, G., Hall, J., Viglione, A., Perdigão, R. A., Parajka, J., Merz, B., . . .
 644 Živković, N. (2019). Changing climate both increases and decreases European
 645 river floods. *Nature*, 573(7772), 108–111. doi: 10.1038/s41586-019-1495-6
- 646 Blöschl, G., Kiss, A., Viglione, A., Barriendos, M., Böhm, O., Brázdil, R., . . . Wet-
 647 ter, O. (2020). Current European flood-rich period exceptional compared with
 648 past 500 years. *Nature*, 583(7817), 560–566. doi: 10.1038/s41586-020-2478-3
- 649 Blöschl, G., & Sivapalan, M. (1995). Scale issues in hydrological modelling: A re-
 650 view. *Hydrological Processes*, 9(3–4), 251–290. doi: 10.1002/hyp.3360090305
- 651 Burn, D. H., & Whitfield, P. H. (2016). Changes in floods and flood regimes
 652 in Canada. *Canadian Water Resources Journal / Revue canadienne des*
 653 *ressources hydriques*, 41(1-2), 139–150. doi: 10.1080/07011784.2015.1026844
- 654 Cao, X., Chen, J., Chen, L. J., Liao, A. P., Sun, F. D., Li, Y., . . . Peng, S.
 655 (2014). Preliminary analysis of spatiotemporal pattern of global land
 656 surface water. *Science China Earth Sciences*, 57(10), 2330–2339. doi:
 657 10.1007/s11430-014-4929-x
- 658 Carabajal, C. C., & Boy, J. P. (2021). Lake and reservoir volume variations in
 659 South America from radar altimetry, ICESat laser altimetry, and GRACE
 660 time-variable gravity. *Advances in Space Research*, 68(2), 652–671. doi:
 661 10.1016/j.asr.2020.04.022
- 662 Chegwiddden, O., Rupp, D. E., & Nijssen, B. (2020, aug). Climate change alters
 663 flood magnitudes and mechanisms in climatically-diverse headwaters across the
 664 northwestern United States. *Environmental Research Letters*, 15(9), 094048.
 665 Retrieved from [https://iopscience.iop.org/article/10.1088/1748-9326/](https://iopscience.iop.org/article/10.1088/1748-9326/ab986fhttps://iopscience.iop.org/article/10.1088/1748-9326/ab986f/meta)
 666 [ab986fhttps://iopscience.iop.org/article/10.1088/1748-9326/ab986f/](https://iopscience.iop.org/article/10.1088/1748-9326/ab986f/meta)
 667 [meta](https://iopscience.iop.org/article/10.1088/1748-9326/ab986f/meta) doi: 10.1088/1748-9326/AB986F
- 668 Cohen, J., Ye, H., & Jones, J. (2015). Trends and variability in rain-on-
 669 snow events. *Geophysical Research Letters*, 42(17), 7115–7122. doi:
 670 10.1002/2015GL065320
- 671 Cramer, V. A., & Hobbs, R. J. (2002). Ecological consequences of altered hy-
 672 drological regimes in fragmented ecosystems in southern Australia: Impacts
 673 and possible management responses. *Austral Ecology*, 27(5), 546–564. doi:
 674 10.1046/j.1442-9993.2002.01215.x
- 675 Cunderlik, J. M., & Ouarda, T. B. (2009). Trends in the timing and magnitude of

- 676 floods in Canada. *Journal of Hydrology*, 375(3-4), 471–480. doi: 10.1016/j
 677 .jhydrol.2009.06.050
- 678 Cunderlik, J. M., Ouarda, T. B. M. J., & Bobée, B. (2004). On the objective identi-
 679 fication of flood seasons. *Water Resources Research*, 40(1), 1–12. doi: 10.1029/
 680 2003WR002295
- 681 Davies, P. M., Bunn, S. E., & Hamilton, S. K. (2008). Primary production in tropi-
 682 cal streams and rivers. In *Tropical stream ecology* (pp. 23–42). Academic Press.
 683 doi: 10.1016/B978-012088449-0.50004-2
- 684 Delgado, J. M., Merz, B., & Apel, H. (2012). A climate-flood link for the lower
 685 Mekong River. *Hydrology and Earth System Sciences*, 16(5), 1533–1541. doi:
 686 10.5194/hess-16-1533-2012
- 687 Do, H. X., Westra, S., Leonard, M., & Gudmundsson, L. (2020). Global-Scale Pre-
 688 diction of Flood Timing Using Atmospheric Reanalysis. *Water Resources Re-
 689 search*, 56(1). doi: 10.1029/2019WR024945
- 690 Fan, Y., Li, H., & Miguez-Macho, G. (2013). Global patterns of groundwater table
 691 depth. *Science*, 339(6122), 940–943. doi: 10.1126/science.1229881
- 692 Favreau, G., Cappelaere, B., Massuel, S., Leblanc, M., Boucher, M., Boulain, N.,
 693 & Leduc, C. (2009). Land clearing, climate variability, and water resources
 694 increase in semiarid southwest Niger: A review. *Water Resources Research*,
 695 45(7), 1–18. doi: 10.1029/2007WR006785
- 696 Faysse, N., Aguilhon, L., Phiboon, K., & Purotaganon, M. (2020). Mainly farming
 697 ... but what’s next? The future of irrigated farms in Thailand. *Journal of Ru-
 698 ral Studies*, 73, 68–76. doi: 10.1016/j.jrurstud.2019.12.002
- 699 Ganguli, P., Nandamuri, Y. R., & Chatterjee, C. (2020). Analysis of persistence
 700 in the flood timing and the role of catchment wetness on flood generation in
 701 a large river basin in India. *Theoretical and Applied Climatology*, 139(1-2),
 702 373–388. doi: 10.1007/s00704-019-02964-z
- 703 Gelmini, Y., Zuecco, G., Zaramella, M., Penna, D., & Borga, M. (2022). Hys-
 704 teresis in streamflow-water table relation provides a new classification sys-
 705 tem of rainfall-runoff events. *Hydrological Processes*, 36(9), e14685. doi:
 706 10.1002/hyp.14685
- 707 Getirana, A., Kumar, S. V., Konapala, G., & Ndehedehe, C. E. (2021). Im-
 708 pacts of Fully Coupling Land Surface and Flood Models on the Simulation
 709 of Large Wetlands’ Water Dynamics: The Case of the Inner Niger Delta. *Jour-
 710 nal of Advances in Modeling Earth Systems*, 13(5), e2021MS002463. doi:
 711 10.1029/2021MS002463
- 712 Giménez, R., Mercau, J. L., Bert, F. E., Kuppel, S., Baldi, G., Houspanossian,
 713 J., ... Jobbágy, E. G. (2020). Hydrological and productive impacts of re-
 714 cent land-use and land-cover changes in the semiarid Chaco: Understanding
 715 novel water excess in water scarce farmlands. *Ecohydrology*, 13(8), 0–3. doi:
 716 10.1002/eco.2243
- 717 Gorelick, N., Hancher, M., Dixon, M., Ilyushchenko, S., Thau, D., & Moore, R.
 718 (2017). Google Earth Engine: Planetary-scale geospatial analysis for everyone.
 719 *Remote Sensing of Environment*, 202, 18–27. doi: 10.1016/j.rse.2017.06.031
- 720 Hall, J., Arheimer, B., Borga, M., Brázdil, R., Claps, P., Kiss, A., ... Blöschl, G.
 721 (2014). Understanding flood regime changes in Europe: A state-of-the-art
 722 assessment. *Hydrology and Earth System Sciences*, 18(7), 2735–2772. doi:
 723 10.5194/hess-18-2735-2014
- 724 Hall, J., & Blöschl, G. (2018). Spatial patterns and characteristics of flood season-
 725 ality in Europe. *Hydrology and Earth System Sciences*, 22(7), 3883–3901. doi:
 726 10.5194/hess-22-3883-2018
- 727 Hartigan, J. A., & Wong, M. A. (1979). Algorithm AS 136: A K-Means Clustering
 728 Algorithm. *Applied Statistics*, 28(1), 100. doi: 10.2307/2346830
- 729 Hayashi, M., van der Kamp, G., & Rosenberry, D. O. (2016). Hydrology of Prairie
 730 Wetlands: Understanding the Integrated Surface-Water and Groundwater

- 731 Processes. *Wetlands*, 36(2), 237–254. doi: 10.1007/s13157-016-0797-9
- 732 Houspanossian, J., Kuppel, S., Nosetto, M. D., Di Bella, C. M., Oricchio, P., Barru-
733 cand, M., . . . Jobbágy, E. G. (2018). Long-lasting floods buffer the thermal
734 regime of the Pampas. *Theoretical and Applied Climatology*, 131(1-2), 111–
735 120. doi: 10.1007/s00704-016-1959-7
- 736 Huang, C., Chen, Y., Zhang, S., & Wu, J. (2018). Detecting, Extracting, and Moni-
737 toring Surface Water From Space Using Optical Sensors: A Review. *Reviews of*
738 *Geophysics*, 56(2), 333–360. doi: 10.1029/2018RG000598
- 739 Huang, J., Pavlic, G., Rivera, A., Palombi, D., & Smerdon, B. (2016). Car-
740 tographier les variations de stock d'eau souterraine avec GRACE: un cas
741 d'étude en Alberta, Canada. *Hydrogeology Journal*, 24(7), 1663–1680. doi:
742 10.1007/s10040-016-1412-0
- 743 Huntington, T. G. (2006). Evidence for intensification of the global water cycle:
744 Review and synthesis. *Journal of Hydrology*, 319(1-4), 83–95. doi: 10.1016/j
745 .jhydrol.2005.07.003
- 746 Ibrakhimov, M., Awan, U. K., George, B., & Liaqat, U. W. (2018). Understanding
747 surface water–groundwater interactions for managing large irrigation schemes
748 in the multi-country Fergana valley, Central Asia. *Agricultural Water Manage-*
749 *ment*, 201, 99–106. doi: 10.1016/j.agwat.2018.01.016
- 750 Jardine, T. D., Bond, N. R., Burford, M. A., Kennard, M. J., Ward, D. P., Bayliss,
751 P., . . . Bunn, S. E. (2015). Does flood rhythm drive ecosystem responses in
752 tropical riverscapes? *Ecology*, 96(3), 684–692. doi: 10.1890/14-0991.1
- 753 Jencso, K. G., & McGlynn, B. L. (2011). Hierarchical controls on runoff generation:
754 Topographically driven hydrologic connectivity, geology, and vegetation. *Water*
755 *Resources Research*, 47(11), 1–16. doi: 10.1029/2011WR010666
- 756 Jin, Q., Wei, J., Yang, Z.-L., & Lin, P. (2017). Irrigation-Induced Environmental
757 Changes around the Aral Sea: An Integrated View from Multiple Satellite
758 Observations. *Remote Sensing*, 9(9), 900. doi: 10.3390/rs9090900
- 759 Jobbágy, E. G., Tóth, T., Nosetto, M. D., & Earman, S. (2017). On the Fundamen-
760 tal Causes of High Environmental Alkalinity (pH>9): An Assessment of Its
761 Drivers and Global Distribution. *Land Degradation and Development*, 28(7),
762 1973–1981. doi: 10.1002/ldr.2718
- 763 Kassambara, A. (2020). *ggpubr: 'ggplot2' based publication ready plots* [software].
764 Retrieved from <https://CRAN.R-project.org/package=ggpubr> (R package
765 version 0.4.0)
- 766 Kassambara, A., & Mundt, F. (2020). *factoextra: Extract and visualize the re-*
767 *sults of multivariate data analyses* [software]. Retrieved from [https://](https://CRAN.R-project.org/package=factoextra)
768 CRAN.R-project.org/package=factoextra (R package version 1.0.7)
- 769 Kemter, M., Marwan, N., Villarini, G., & Merz, B. (2023, jan). Controls on Flood
770 Trends Across the United States. *Water Resources Research*, e2021WR031673.
771 Retrieved from [https://onlinelibrary.wiley.com/doi/full/10.1029/](https://onlinelibrary.wiley.com/doi/full/10.1029/2021WR031673)
772 [https://onlinelibrary.wiley.com/doi/abs/10.1029/](https://onlinelibrary.wiley.com/doi/abs/10.1029/2021WR031673)
773 [https://agupubs.onlinelibrary.wiley.com/doi/10.1029/](https://agupubs.onlinelibrary.wiley.com/doi/10.1029/2021WR031673)
774 [2021WR031673](https://agupubs.onlinelibrary.wiley.com/doi/10.1029/2021WR031673) doi: 10.1029/2021WR031673
- 775 Knox, J. C. (2000). Sensitivity of modern and Holocene floods to climate change. In
776 *Quaternary science reviews* (Vol. 19, pp. 439–457). Pergamon. doi: 10.1016/
777 S0277-3791(99)00074-8
- 778 Komsta, L., & Novomestky, F. (2015). *moments: Moments, cumulants, skewness,*
779 *kurtosis and related tests* [software]. Retrieved from [https://CRAN.R-project](https://CRAN.R-project.org/package=moments)
780 [.org/package=moments](https://CRAN.R-project.org/package=moments) (R package version 0.14)
- 781 Kottek, M., Grieser, J., Beck, C., Rudolf, B., & Rubel, F. (2006a). [dataset]. Re-
782 trieved from <http://koeppen-geiger.vu-wien.ac.at/present.htm> doi: 10
783 .1127/0941-2948/2006/0130
- 784 Kottek, M., Grieser, J., Beck, C., Rudolf, B., & Rubel, F. (2006b). World Map of
785 the Köppen-Geiger climate classification updated. *Meteorologische Zeitschrift*,

- 786 15(3), 259–263. doi: 10.1127/0941-2948/2006/0130
- 787 Krinner, G. (2003). Impact of lakes and wetlands on boreal climate. *Journal of Geo-*
788 *physical Research: Atmospheres*, 108(16), 4520. doi: 10.1029/2002jd002597
- 789 Kumar, L., & Mutanga, O. (2018). Google Earth Engine Applications Since Incep-
790 tion: Usage, Trends, and Potential. *Remote Sensing*, 10(10), 1509. doi: 10
791 .3390/rs10101509
- 792 Kundzewicz, Z. W., Szwed, & Pińskwar. (2019). Climate Variability and Floods—A
793 global Review. *Water*, 11(7), 1399. doi: 10.3390/w11071399
- 794 Kuppel, S., Houspanossian, J., Noretto, M. D., & Jobbágy, E. G. (2015). What
795 does it take to flood the Pampas?: Lessons from a decade of strong hydro-
796 logical fluctuations. *Water Resources Research*, 51(4), 2937–2950. doi:
797 10.1002/2015WR016966
- 798 Lee, D., Ward, P., & Block, P. (2015). Defining high-flow seasons using tempo-
799 ral streamflow patterns from a global model. *Hydrology and Earth System Sci-*
800 *ences*, 19(11), 4689–4705. doi: 10.5194/hess-19-4689-2015
- 801 Liu, D., Wang, Z., Song, K., Zhang, B., Hu, L., Huang, N., . . . Jiang, G. (2009).
802 Land use/cover changes and environmental consequences in Songnen Plain,
803 Northeast China. *Chinese Geographical Science*, 19(4), 299–305. doi:
804 10.1007/s11769-009-0299-2
- 805 Loarie, S. R., Lobell, D. B., Asner, G. P., & Field, C. B. (2011). Land-Cover and
806 Surface Water Change Drive Large Albedo Increases in South America*. *Earth*
807 *Interactions*, 15(7), 1–16. doi: 10.1175/2010EI342.1
- 808 Lopez, T., Al Bitar, A., Biancamaria, S., Güntner, A., & Jäggi, A. (2020). *On the*
809 *Use of Satellite Remote Sensing to Detect Floods and Droughts at Large Scales*
810 (Vol. 41) (No. 6). Springer. doi: 10.1007/s10712-020-09618-0
- 811 McCabe, G. J., Clark, M. P., & Hay, L. E. (2007). Rain-on-snow events in the
812 western United States. *Bulletin of the American Meteorological Society*, 88(3),
813 319–328. doi: 10.1175/BAMS-88-3-319
- 814 McLeod, A. (2022). *Kendall: Kendall rank correlation and mann-kendall trend test*
815 [software]. Retrieved from <https://CRAN.R-project.org/package=Kendall>
816 (R package version 2.2.1)
- 817 Meriö, L., Ala-aho, P., Linjama, J., Hjort, J., Kløve, B., & Marttila, H. (2019).
818 Snow to Precipitation Ratio Controls Catchment Storage and Summer Flows
819 in Boreal Headwater Catchments. *Water Resources Research*, 2018WR023031.
820 doi: 10.1029/2018WR023031
- 821 Merz, B., Blöschl, G., Vorogushyn, S., Dottori, F., Aerts, J. C., Bates, P., . . . Mac-
822 donald, E. (2021). *Causes, impacts and patterns of disastrous river floods*
823 (Vol. 2) (No. 9). Nature Publishing Group. doi: 10.1038/s43017-021-00195-3
- 824 Merz, R., & Blöschl, G. (2003). A process typology of regional floods. *Water Re-*
825 *sources Research*, 39(12), 1340. doi: 10.1029/2002WR001952
- 826 Micklin, P. (1988). Desiccation of the Aral Sea: A Water Management Disaster in
827 the Soviet Union. *Science*, 241, 1170–76.
- 828 Microsoft Corporation, & Weston, S. (2020a). *doparallel: Foreach parallel adaptor*
829 *for the 'parallel' package* [software]. Retrieved from [https://CRAN.R-project](https://CRAN.R-project.org/package=doParallel)
830 [.org/package=doParallel](https://CRAN.R-project.org/package=doParallel) (R package version 1.0.16)
- 831 Microsoft Corporation, & Weston, S. (2020b). *foreach: Provides foreach looping*
832 *construct* [software]. Retrieved from [https://CRAN.R-project.org/package=](https://CRAN.R-project.org/package=foreach)
833 [foreach](https://CRAN.R-project.org/package=foreach) (R package version 1.5.1)
- 834 Miguez-Macho, G., & Fan, Y. (2012). The role of groundwater in the Amazon
835 water cycle: 1. Influence on seasonal streamflow, flooding and wetlands.
836 *Journal of Geophysical Research: Atmospheres*, 117(D15), n/a–n/a. doi:
837 10.1029/2012JD017539
- 838 O'Neill, R. V., Deangelis, D. L., Waide, J. B., Allen, T. F., & Allen, G. E. (1986). *A*
839 *hierarchical concept of ecosystems*. Princeton University Press.
- 840 Papa, F., Frappart, F., Güntner, A., Prigent, C., Aires, F., Getirana, A., & Maurer,

- 841 R. (2013). Surface freshwater storage and variability in the Amazon basin
842 from multi-satellite observations, 1993-2007. *Journal of Geophysical Research*
843 *Atmospheres*, 118(21), 11951–11965. doi: 10.1002/2013JD020500
- 844 Parajka, J., Kohnová, S., Bálint, G., Barbuc, M., Borga, M., Claps, P., ...
845 Blöschl, G. (2010). Seasonal characteristics of flood regimes across the
846 Alpine-Carpathian range. *Journal of Hydrology*, 394(1-2), 78–89. doi:
847 10.1016/j.jhydrol.2010.05.015
- 848 Pebesma, E. (2018). *Simple Features for R: Standardized Support for Spatial Vector*
849 *Data* (Vol. 10) (software No. 1). Retrieved from [https://doi.org/10.32614/](https://doi.org/10.32614/RJ-2018-009)
850 [RJ-2018-009](https://doi.org/10.32614/RJ-2018-009) doi: 10.32614/RJ-2018-009
- 851 Pekel, J.-F., Cottam, A., Gorelick, N., & Belward, A. S. (2016a). High-resolution
852 mapping of global surface water and its long-term changes. *Nature*, 540(7633),
853 418–422. doi: 10.1038/nature20584
- 854 Pekel, J.-F., Cottam, A., Gorelick, N., & Belward, A. S. (2016b). *High-resolution*
855 *mapping of global surface water and its long-term changes* [dataset]. Na-
856 ture Publishing Group. Retrieved from [https://developers.google.com/](https://developers.google.com/earth-engine/datasets/catalog/JRC_GSW1_4_MonthlyHistory)
857 [earth-engine/datasets/catalog/JRC_GSW1_4_MonthlyHistory](https://developers.google.com/earth-engine/datasets/catalog/JRC_GSW1_4_MonthlyHistory) doi:
858 10.1038/nature20584
- 859 Pickens, A. H., Hansen, M. C., Hancher, M., Stehman, S. V., Tyukavina, A.,
860 Potapov, P., ... Sherani, Z. (2020). Mapping and sampling to character-
861 ize global inland water dynamics from 1999 to 2018 with full Landsat time-
862 series. *Remote Sensing of Environment*, 243(December 2019), 111792. doi:
863 10.1016/j.rse.2020.111792
- 864 Prigent, C., Papa, F., Aires, F., Rossow, W. B., & Matthews, E. (2007). Global
865 inundation dynamics inferred from multiple satellite observations, 1993-2000.
866 *Journal of Geophysical Research Atmospheres*, 112(12), 1993–2000. doi:
867 10.1029/2006JD007847
- 868 R Core Team. (2021a). *R: A language and environment for statistical computing*
869 [software]. Vienna, Austria. Retrieved from <https://www.R-project.org/>
- 870 R Core Team. (2021b). *R: A language and environment for statistical computing*
871 [software]. Vienna, Austria. Retrieved from <https://www.R-project.org/>
- 872 Raymaekers, J. (2022). *robslopes: Fast algorithms for robust slopes* [software]. Re-
873 trieved from <https://CRAN.R-project.org/package=robslopes> (R package
874 version 1.1.2)
- 875 Reager, J. T., Thomas, B. F., & Famiglietti, J. S. (2014). River basin flood potential
876 inferred using GRACE gravity observations at several months lead time. *Na-*
877 *ture Geoscience*, 7(8), 588–592. doi: 10.1038/ngeo2203
- 878 Robertson, A. I., Bacon, P., & Heagney, G. (2001). The responses of floodplain
879 primary production to flood frequency and timing. *Journal of Applied Ecology*,
880 38(1), 126–136. doi: 10.1046/j.1365-2664.2001.00568.x
- 881 Roebroek, C. T. J. (2020). *Global distribution of hydrologic controls on forest growth*
882 [dataset]. HydroShare. Retrieved from [https://www.hydroshare.org/](https://www.hydroshare.org/resource/38ac7dd90c7d4353bb492604981782f0)
883 [resource/38ac7dd90c7d4353bb492604981782f0](https://www.hydroshare.org/resource/38ac7dd90c7d4353bb492604981782f0) doi: [https://doi.org/](https://doi.org/10.4211/hs.38ac7dd90c7d4353bb492604981782f0)
884 [10.4211/hs.38ac7dd90c7d4353bb492604981782f0](https://doi.org/10.4211/hs.38ac7dd90c7d4353bb492604981782f0)
- 885 Roebroek, C. T. J., Melsen, L. A., Hoek van Dijke, A. J., Fan, Y., & Teul-
886 ing, A. J. (2020). Global distribution of hydrologic controls on forest
887 growth. *Hydrology and Earth System Sciences*, 24(9), 4625–4639. doi:
888 10.5194/hess-24-4625-2020
- 889 Rogger, M., Agnoletti, M., Alaoui, A., Bathurst, J. C., Bodner, G., Borga, M., ...
890 Blöschl, G. (2017). *Land use change impacts on floods at the catchment scale: Challenges and opportunities for future research* (Vol. 53) (No. 7). John Wiley
891 & Sons, Ltd. doi: 10.1002/2017WR020723
- 892
893 Rojas, F., Rubio, C., Rizzo, M., Bernabeu, M., Akil, N., & Martín, F. (2020). Land
894 Use and Land Cover in Irrigated Drylands: a Long-Term Analysis of Changes
895 in the Mendoza and Tunuyán River Basins, Argentina (1986–2018). *Applied*

- 896 *Spatial Analysis and Policy*, 13(4), 875–899. doi: 10.1007/s12061-020-09335-6
- 897 Rubel, F., Brugger, K., Haslinger, K., & Auer, I. (2017). The climate of the Eu-
898 ropean Alps: Shift of very high resolution Köppen-Geiger climate zones 1800-
899 2100. *Meteorologische Zeitschrift*, 26(2), 115–125. doi: 10.1127/metz/2016/
900 0816
- 901 Saharia, M., Kirstetter, P. E., Vergara, H., Gourley, J. J., & Hong, Y. (2017).
902 Characterization of floods in the United States. *Journal of Hydrology*, 548,
903 524–535. doi: 10.1016/j.jhydrol.2017.03.010
- 904 Sanchis, E., Ferrer, M., Torres, A. G., Cambra-López, M., & Calvet, S. (2012). Ef-
905 fect of Water and Straw Management Practices on Methane Emissions from
906 Rice Fields: A Review Through a Meta-Analysis. *Environmental Engineering
907 Science*, 29(12), 1053–1062. doi: 10.1089/ees.2012.0006
- 908 Schrapffer, A., Sörensson, A., Polcher, J., & Fita, L. (2020). Benefits of repre-
909 senting floodplains in a Land Surface Model: Pantanal simulated with OR-
910 CHIDEE CMIP6 version. *Climate Dynamics*, 55(5-6), 1303–1323. doi:
911 10.1007/s00382-020-05324-0
- 912 Scordo, F., Bohn, V. Y., Piccolo, M. C., & Perillo, G. M. (2018). Mapping and
913 monitoring Lakes Intra-Annual variability in semi-arid regions: A case of study
914 in Patagonian Plains (Argentina). *Water (Switzerland)*, 10(7), 889. doi:
915 10.3390/w10070889
- 916 Sen, P. K. (1968). Estimates of the Regression Coefficient Based on Kendall’s Tau.
917 *Journal of the American Statistical Association*, 63(324), 1379–1389. doi: 10
918 .1080/01621459.1968.10480934
- 919 Silva, A. T., Portela, M. M., Naghettini, M., & Fernandes, W. (2017). A Bayesian
920 peaks-over-threshold analysis of floods in the Itajaí-açu River under stationar-
921 ity and nonstationarity. *Stochastic Environmental Research and Risk Assess-
922 ment*, 31(1), 185–204. doi: 10.1007/s00477-015-1184-4
- 923 Simões, N. R., Dias, J. D., Leal, C. M., de Souza Magalhães Braghin, L., Lansac-
924 Tôha, F. A., & Bonecker, C. C. (2013). Floods control the influence of environ-
925 mental gradients on the diversity of zooplankton communities in a neotropical
926 floodplain. *Aquatic Sciences*, 75(4), 607–617. doi: 10.1007/s00027-013-0304-9
- 927 Sivapalan, M. (2005). Pattern, Process and Function: Elements of a Unified Theory
928 of Hydrology at the Catchment Scale. In *Encyclopedia of hydrological sciences*.
929 John Wiley & Sons, Ltd. doi: 10.1002/0470848944.hsa012
- 930 Song, C., Huang, B., Richards, K., Ke, L., & Hien Phan, V. (2014). Accelerated
931 lake expansion on the Tibetan Plateau in the 2000s: Induced by glacial melt-
932 ing or other processes? *Water Resources Research*, 50(4), 3170–3186. doi:
933 10.1002/2013WR014724
- 934 Statisticat, & LLC. (2021). *Laplacedemon tutorial* [software]. Bayesian-
935 Inference.com. Retrieved from [https://web.archive.org/web/
936 20150206004624/http://www.bayesian-inference.com/software](https://web.archive.org/web/20150206004624/http://www.bayesian-inference.com/software) (R
937 package version 16.1.6)
- 938 Stein, L., Pianosi, F., & Woods, R. (2020). Event-based classification for global
939 study of river flood generating processes. *Hydrological Processes*, 34(7), 1514–
940 1529. doi: 10.1002/hyp.13678
- 941 Stewart, I. T., Cayan, D. R., & Dettinger, M. D. (2005). Changes toward earlier
942 streamflow timing across western North America. *Journal of Climate*, 18(8),
943 1136–1155. doi: 10.1175/JCLI3321.1
- 944 Tapley, B. D., Bettadpur, S., Ries, J. C., Thompson, P. F., & Watkins, M. M.
945 (2004). GRACE Measurements of Mass Variability in the Earth System.
946 *Science*, 305(5683), 503–505. doi: 10.1126/science.1099192
- 947 Tapley, B. D., Watkins, M. M., Flechtner, F., Reigber, C., Bettadpur, S., Rodell,
948 M., . . . Velicogna, I. (2019). Contributions of GRACE to understand-
949 ing climate change. *Nature Climate Change*, 9(5), 358–369. doi: 10.1038/
950 s41558-019-0456-2

- 951 Theil, H. (1992). A Rank-Invariant Method of Linear and Polynomial Regression
 952 Analysis. In (pp. 345–381). Springer, Dordrecht. doi: 10.1007/978-94-011-2546
 953 -8.20
- 954 Torre Zaffaroni, P., Baldi, G., Texeira, M., Di Bella, C. M., & Jobbágy, E. G. (2022,
 955 jun). *The Timing of Global Floods and its Association with Climate and Topo-*
 956 *graphy - associated Data and Codes* [software]. Zenodo. doi: 10.5281/zenodo
 957 .7328786
- 958 Tramblay, Y., Villarini, G., El Khalki, E. M., Gründemann, G., & Hughes, D. (2021,
 959 jun). Evaluation of the Drivers Responsible for Flooding in Africa. *Water*
 960 *Resources Research*, 57(6), e2021WR029595. Retrieved from [https://](https://onlinelibrary.wiley.com/doi/full/10.1029/2021WR029595)
 961 onlinelibrary.wiley.com/doi/full/10.1029/2021WR029595[https://](https://onlinelibrary.wiley.com/doi/abs/10.1029/2021WR029595)
 962 onlinelibrary.wiley.com/doi/abs/10.1029/2021WR029595[https://](https://agupubs.onlinelibrary.wiley.com/doi/10.1029/2021WR029595)
 963 agupubs.onlinelibrary.wiley.com/doi/10.1029/2021WR029595 doi:
 964 10.1029/2021WR029595
- 965 Trenberth, K. E. (2011). Changes in precipitation with climate change. *Climate Re-*
 966 *search*, 47(1-2), 123–138. doi: 10.3354/cr00953
- 967 Troch, P. A., Smith, J. A., Wood, E. F., & de Troch, F. P. (1994). Hydrologic con-
 968 trols of large floods in a small basin: central Appalachian case study. *Journal*
 969 *of Hydrology*, 156(1-4), 285–309. doi: 10.1016/0022-1694(94)90082-5
- 970 Tulbure, M. G., & Broich, M. (2019). Spatiotemporal patterns and effects of climate
 971 and land use on surface water extent dynamics in a dryland region with three
 972 decades of Landsat satellite data. *Science of the Total Environment*, 658,
 973 1574–1585. doi: 10.1016/j.scitotenv.2018.11.390
- 974 Verbesselt, J., Hyndman, R., Newnham, G., & Culvenor, D. (2010). Detecting trend
 975 and seasonal changes in satellite image time series. *Remote Sensing of Envi-*
 976 *ronment*, 114(1), 106–115. doi: 10.1016/j.rse.2009.08.014
- 977 Viglione, A., Merz, B., Viet Dung, N., Parajka, J., Nester, T., & Blöschl, G. (2016).
 978 Attribution of regional flood changes based on scaling fingerprints. *Water Re-*
 979 *sources Research*, 52(7), 5322–5340. doi: 10.1002/2016WR019036
- 980 Viglizzo, E. F., Frank, F. C., Carreño, L. V., Jobbágy, E. G., Pereyra, H., Clatt, J.,
 981 ... Ricard, M. F. (2011). Ecological and environmental footprint of 50 years
 982 of agricultural expansion in Argentina. *Global Change Biology*, 17(2), 959–973.
 983 doi: 10.1111/j.1365-2486.2010.02293.x
- 984 Villarini, G. (2016). On the seasonality of flooding across the continental United
 985 States. *Advances in Water Resources*, 87, 80–91. doi: 10.1016/j.advwatres
 986 .2015.11.009
- 987 Vormoor, K., Lawrence, D., Heistermann, M., & Bronstert, A. (2015). Climate
 988 change impacts on the seasonality and generation processes of floods –
 989 Projections and uncertainties for catchments with mixed snowmelt/rainfall
 990 regimes. *Hydrology and Earth System Sciences*, 19(2), 913–931. doi:
 991 10.5194/hess-19-913-2015
- 992 Wang, Z., Song, K., Zhang, B., Liu, D., Ren, C., Luo, L., ... Liu, Z. (2009). Shrink-
 993 age and fragmentation of grasslands in the West Songnen Plain, China. *Agri-*
 994 *culture, Ecosystems and Environment*, 129(1-3), 315–324. doi: 10.1016/j.agee
 995 .2008.10.009
- 996 Wang, Z., & Vivoni, E. R. (2022). Individualized and Combined Effects of Future
 997 Urban Growth and Climate Change on Irrigation Water Use in Central Ari-
 998 zona. *Journal of the American Water Resources Association*, 58(3), 370–387.
 999 doi: 10.1111/1752-1688.13005
- 1000 Warfe, D. M., Pettit, N. E., Davies, P. M., Pusey, B. J., Hamilton, S. K., Ken-
 1001 nard, M. J., ... Halliday, I. A. (2011). *The 'wet-dry' in the wet-dry tropics*
 1002 *drives river ecosystem structure and processes in northern Australia* (Vol. 56)
 1003 (No. 11). John Wiley & Sons, Ltd. doi: 10.1111/j.1365-2427.2011.02660.x
- 1004 Wasko, C., Nathan, R., & Peel, M. C. (2020a, mar). Changes in Antecedent Soil
 1005 Moisture Modulate Flood Seasonality in a Changing Climate. *Water Resources*

- 1006 *Research*, 56(3), no. Retrieved from <https://onlinelibrary.wiley.com/doi/full/10.1029/2019WR026300>
1007 <https://onlinelibrary.wiley.com/doi/abs/10.1029/2019WR026300>
1008 <https://agupubs.onlinelibrary.wiley.com/doi/10.1029/2019WR026300> doi: 10.1029/2019WR026300
1009
1010 Wasko, C., Nathan, R., & Peel, M. C. (2020b). Trends in Global Flood and Stream-
1011 flow Timing Based on Local Water Year. *Water Resources Research*, 56(8), 0–
1012 2. doi: 10.1029/2020WR027233
1013 Whitworth, K. L., Baldwin, D. S., & Kerr, J. L. (2012). Drought, floods and wa-
1014 ter quality: Drivers of a severe hypoxic blackwater event in a major river
1015 system (the southern Murray-Darling Basin, Australia). *Journal of Hy-*
1016 *drology*, 450-451, 190–198. Retrieved from [http://dx.doi.org/10.1016/](http://dx.doi.org/10.1016/j.jhydrol.2012.04.057)
1017 [j.jhydrol.2012.04.057](http://dx.doi.org/10.1016/j.jhydrol.2012.04.057) doi: 10.1016/j.jhydrol.2012.04.057
1018 Wickham, H. (2016). *ggplot2: Elegant graphics for data analysis* [software]. Springer-
1019 Verlag New York. Retrieved from <https://ggplot2.tidyverse.org>
1020 Wickham, H. (2021). *tidyr: Tidy messy data* [software]. Retrieved from [https://](https://CRAN.R-project.org/package=tidyr)
1021 CRAN.R-project.org/package=tidyr (R package version 1.1.4)
1022 Woldemeskel, F., & Sharma, A. (2016). Should flood regimes change in a warming
1023 climate? The role of antecedent moisture conditions. *Geophysical Research Let-*
1024 *ters*, 43(14), 7556–7563. doi: 10.1002/2016GL069448
1025 Yang, K., Wu, H., Qin, J., Lin, C., Tang, W., & Chen, Y. (2014). Recent cli-
1026 mate changes over the Tibetan Plateau and their impacts on energy and
1027 water cycle: A review. *Global and Planetary Change*, 112, 79–91. doi:
1028 [10.1016/j.gloplacha.2013.12.001](https://doi.org/10.1016/j.gloplacha.2013.12.001)
1029 Yang, L., Yang, Y., Villarini, G., Li, X., Hu, H., Wang, L., ... Tian, F. (2021).
1030 Climate More Important for Chinese Flood Changes Than Reservoirs and
1031 Land Use. *Geophysical Research Letters*, 48(11), e2021GL093061. doi:
1032 [10.1029/2021GL093061](https://doi.org/10.1029/2021GL093061)
1033 Zhang, S., Zhou, L., Zhang, L., Yang, Y., Wei, Z., Zhou, S., ... Dai, Y. (2022,
1034 nov). Reconciling disagreement on global river flood changes in a warm-
1035 ing climate. *Nature Climate Change* 2022 12:12, 12(12), 1160–1167. Re-
1036 trieved from <https://www.nature.com/articles/s41558-022-01539-7> doi:
1037 [10.1038/s41558-022-01539-7](https://doi.org/10.1038/s41558-022-01539-7)
1038 Zhang, Y., Zang, S., Sun, L., Yan, B., Yang, T., Yan, W., ... Qi, J. (2019). Charac-
1039 terizing the changing environment of cropland in the Songnen Plain, Northeast
1040 China, from 1990 to 2015. *Journal of Geographical Sciences*, 29(5), 658–674.
1041 doi: 10.1007/s11442-019-1620-3
1042 Zuecco, G., Penna, D., Borga, M., & van Meerveld, H. J. (2016). A versatile index
1043 to characterize hysteresis between hydrological variables at the runoff event
1044 timescale. *Hydrological Processes*, 30(9), 1449–1466. doi: 10.1002/hyp.10681